GeoScienceWorld
Lithosphere
Volume 2021, Article ID 8836546, 18 pages
https://doi.org/10.2113/2021/8836546

Lithosphere

Research Article

Posteruptive Thermal History of the Proterozoic Basaltic North Shore Volcanic Group of the Midcontinent Rift: Evidence from K/Ar Data of Celadonite

Susanne Theodora Schmidt,[1] **Annette Süssenberger**,[1] **and Klaus Wemmer**[2]

[1]*Department of Earth Sciences, Université de Genève, Rue des Maraîchers 13, 1205 Genève, Switzerland*
[2]*Geowissenschaftliches Zentrum der Georg-August-Universität, Goldschmidtstr. 3, 37077 Göttingen, Germany*

Correspondence should be addressed to Susanne Theodora Schmidt; susanne.schmidt@unige.ch

Received 12 March 2020; Accepted 1 October 2020; Published 27 February 2021

Academic Editor: Matt Steele-MacInnes

This study reports three K/Ar ages on celadonite, a dioctahedral K-Fe mica, in the Proterozoic North Shore Volcanic Group (NSVG) of the Midcontinent Rift in northeastern Minnesota. Celadonite formed during beginning posteruptive, low-temperature conditions at temperatures < 100°C and with input of meteoric water. K/Ar ages between 1062 ± 16 Ma and 955.0 ± 12 Ma document a remarkably long posteruptive thermal history of >100 myrs in a thick continental basaltic sequence. In the stratigraphically lower part of the NSVG, celadonite formation occurred at 1062 ± 16 Ma in an amygdule or a vesicle filled with celadonite, while another celadonite amygdule in a stratigraphically higher flow was dated at 1039.4 ± 14 Ma. Both flows are overprinted by a later multistage lower zeolite-phyllosilicate facies assemblage (laumontite-albite-corrensite±chlorite±smectite ±prehnite±pumpellyite). In the stratigraphically higher part of the sequence, celadonite crystallization at an amygdule rim is followed by upper zeolite facies conditions (stilbite-heulandite-smectite assemblage) and was dated at 955.0 ± 12.4 Ma. The constrained time frame of 107 myrs indicates a long-lived, probably not continuous and locally occurring, posteruptive thermal alteration process. The data suggest that alteration was depth-controlled and temporally and spatially inhomogeneous and implies the progression of the sequence from a close-to-the-surface alteration mode with input of meteoric water to a burial metamorphic mode and with locally occurring hydrothermal activity due to continuous magmatic activity. Volcanism in the Midcontinent Rift system is supposed to have lasted between 1109 Ma and 1083 Ma based on U/Pb zircon ages. The first crystallization of celadonite is recorded in the lower part of the NSVG and occurred ca. 30 myrs after the emplacement of the Silver Bay aplite intrusion in the upper part of the NSVG. Burial rates are determined to be 0.04 km·Ma^{-1}and 0.10 km·Ma^{-1}. The hydrothermal alteration under low-temperature burial conditions clearly postdates the rift-related alkaline and tholeiitic magmatism of the Midcontinent Rift and overlaps with the depositional window of the sedimentary rocks that overlie the Midcontinent Rift volcanics, as well as crustal-scale fault systems that were active during Grenvillian tectonic uplift after the cessation of magmatic activity.

1. Introduction

Hydrothermal alteration of basalts is a widespread phenomenon and has been documented from recent and ancient ocean floor basalts such as the Reykjanes Peninsula in western Iceland [1], the Deep Sea Drilling Project (DSDP) Leg 37 from the western flank of the Atlantic Ridge [2], the ODP Site 1001 Leg 165 from Cretaceous basalts from the Caribbean Sea [3], the eastern flank of the Juan de Fuca Ridge at 48°N [4], or the Oman ophiolite [5]. Detailed correlation of observed mineral assemblages with measured temperatures (e.g., [6–8]) has established a framework of temperatures to estimate conditions in extinct hydrothermal systems. However, constraints on the onset and duration of the posteruptive thermal history in thick basaltic sequences are difficult to obtain. Dating the alteration events is not a straightforward task due to the scarcity of datable minerals recording later thermal events. A datable mineral is

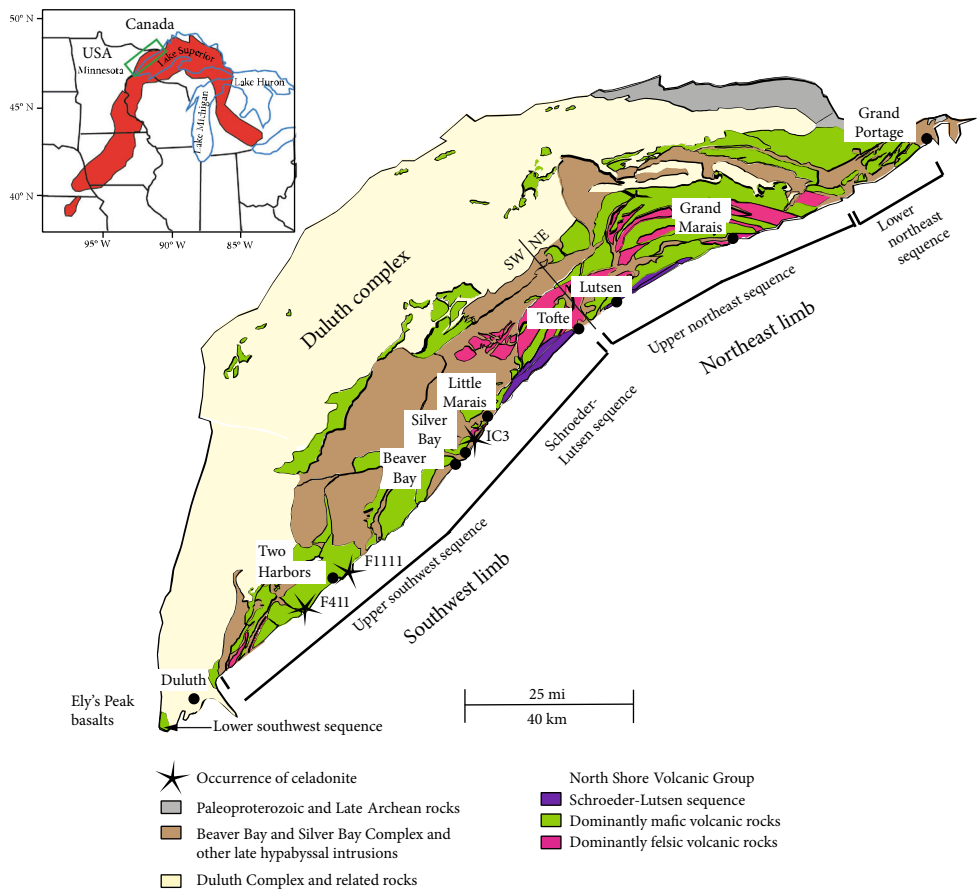

FIGURE 1: Location and general geology of the Midcontinent Rift and the North Shore Volcanic Group with the sample locations of celadonite in flows IC3, F411, and F1111 based on Green et al. [24] and Miller et al. [90]. Inlet figure: outline of the rocks of the Midcontinent Rift (volcanic and clastic sedimentary rocks) with the location of the study area (green rectangle) according to the gravity map of Stein et al. [91].

celadonite, a dioctahedral K-bearing mica, well-known as a low-temperature alteration phase within the oceanic crust (e.g., [9]). We applied conventional K-Ar dating on celadonite, although neither a closing temperature nor data on the retentivity of argon are known. Due to the structural similarity to glauconite, a similar behavior can be assumed concerning the K-Ar system of celadonite. Glauconite has proven to be very suitable for age dating in prograde diagenetic evolution up to deep diagenesis (e.g., [10]). Clauer et al. [11] and Kowalska et al. [12] have compared K-Ar and Ar/Ar techniques and confirmed the high reliability of K-Ar data for clay-size minerals.

Celadonite is a characteristic bluish-green to greenish mica with the general formula $K(Mg,Fe^{2+})(Fe^{3+},Al)Si_4O_{10}(OH)_2$ [9]. Its occurrence has been often described in vesicles of deep-sea floor basalts from various ocean drilling legs (e.g., [7, 13, 14]). It is found in the Troodos Massif in Cyprus [15], where it occurs in the low-temperature alteration zone, and in mafic Triassic volcanic rocks of the external Hellenides of western Greece [16]. Its genesis in the marine environment of the oceanic crust is generally linked to low-temperature hydrothermal conditions of $T < 120°C$ and is mainly controlled by access of seawater and chemical parameters such as pH or fO_2. Celadonite is also known in Iceland from the Late Tertiary to Early Quarternary flood basalts in the Hvalfjördur area [17] and at Teigarhorn [18] where it formed at shallow depths close to the surface at temperatures around 50°C and at the beginning of burial metamorphism. Celadonite occurs also in the continental flood basalts of the Miocene Grande Ronde Basalts of the Columbia River Basalt Group in Washington [19] where it crystallized slowly at temperatures between 15 and 35°C, with oxygen fugacity buffered by interaction with basalt and related to the Grande Ronde Aquifer. It is also reported in the flood basalts from the Deccan Traps Volcanic Province by Ottens al. [20] as first rim-forming mineral in cavities. It also occurs in the Tertiary basalts of the Lessini Mountains of northern Italy where it is assumed to have crystallized during the deuteric cooling stage from a residual fluid with H_2O and fluids [21]. It is also documented in soil where it is the weathering product of Lower Carboniferous basalts in the Lake District in England [22]. It is also detected on Mars [23].

The studied celadonites occur in amygdules of subaerial basalts in the Proterozoic North Shore Volcanic Group (NSVG) of northeastern Minnesota related to the Midcontinent Rift within the North American Craton. The Southwest Limb of the NSVG (for a summary, see [24]) has an approximate thickness of 9735 m between Duluth and Tofte (Figure 1). It experienced metamorphic conditions with upper zeolite facies conditions in the stratigraphically upper

part which reached up to upper greenschist facies conditions in the lower part of the section [25–27]. Celadonite has been reported to occur in three lava flows partly replacing olivine and rimming amygdules throughout the sequence [25]. It is the aim of this study to date the beginning posteruptive thermal alteration event as expressed in the formation of celadonite. Age determination of celadonite records a maximum age of low-temperature alteration, because it is an early crystallized alteration phase at close-to-surface conditions. Alteration proceeds with later burial alteration assemblages of increasingly higher temperature and local hydrothermal alteration.

2. Geological Background

2.1. The Midcontinent Rift and the North Shore Volcanic Group. The ca. 1.1 Ga Midcontinent Rift is a 2500 km long mafic-dominated continental rift system within the North American Craton ([24, 28–34]Figure 1). It is traditionally considered to be an example of a failed rift attributed to a plume-related thermal anomaly in the mantle [35] as the result of the compressional effect of the Grenville orogeny to the East [36]. Stein et al. [31] and Stein et al. [30] suggested that it is a remnant part of the rifting event between Amazonia (Precambrian northeast South America) and Laurentia (Precambrian North America). Swanson-Hysell et al. [34] relate the prolonged magmatism of the Midcontinent Rift to the fast plate motion of Laurentia associated with an avalanche of subducted slab material. Magmatic activity of the Midcontinent Rift is documented from 1109 Ma to 1083 Ma or equivalent to a time span of approximately 25 myrs [24, 33, 34, 37–40]. In northeastern Minnesota, the Midcontinent Rift comprises the NSVG which is one of several plateau lava sequences consisting of volcanic rocks and interbedded sediments [24, 41–43]. The NSVG is well exposed along the shoreline of Lake Superior and is slightly tilted towards the southeast, i.e., towards the axis of the Midcontinent Rift. It is intruded by comagmatic and coeval plutonic and associated hypabyssal rocks, predominantly the Duluth Complex and the Beaver Bay Complex ([24, 33, 34, 44]; Figures 1 and 2). Gustavson [45] calculated a geothermal gradient of 40°C/km based on temperature differences of zeolite assemblages in two flows in the upper part of the sequence. Using the phyllosilicate assemblages of Schmidt and Robinson [27], a lower geothermal gradient of 25°C/km is determined. Interbedded sedimentary rocks within the NSVG such as sandstone, breccia, and shale suggest a terrestrial deposition environment of braided streams [43].

The NSVG (Figure 2) consists of a Northeast Limb (N of Lutsen to Grand Portage) and a Southwest limb (SW of Tofte) which are subdivided into formational units [24]. This study focuses on the Southwest Limb between Tofte and Duluth (Figures 1 and 2). Characteristic outcrop features and alteration minerals of the NSVG are shown in Figure 3. Contacts between flows are well recognized in the field (Figure 3(a)), Pahoehoe textures are still preserved (Figure 3(b)), and terrestrial sediments witness the general subaerial character of the sequence (Figure 3(c)). The Southwest Limb (SW of Tofte) of the NSVG has an approximate thickness of 9735 m [24] and experienced a posteruptive depth-controlled multistage low-temperature alteration history with locally occurring hydrothermal alteration and a distinct metamorphic facies pattern (Figure 2; [25–27, 45]). These depth-related characteristic mineral assemblages reflect the developing multistage thermal history and did not necessarily precipitate simultaneously. Rather, they crystallized sequentially as evident from the amygdule mineral sequence or the crystallization of minerals from the rim to the center of amygdules (Figure 4). However, in stratigraphically lower flows, this mineral sequence might be occasionally reversed with assemblages of higher temperature replacing assemblages of lower temperature along amygdule rims. Following the shoreline from the village of Tofte to the city of Duluth in the southwest, the basaltic sequence becomes successively older (Figures 1 and 2). Based on amygdule mineral assemblages and alteration of magmatic constituents (olivine, clinopyroxene, orthopyroxene, plagioclase, and FeO-Ti-oxides), the metamorphic grade reaches from upper zeolite facies conditions (thomsonite±mesolite±-scolecite-smectite, Figures 3(d) and 4(a)–4(c), and heulandite-stilbite-smectite±laumontite, Figures 3(e)–3(h), 3(n), and 4(d)) in the stratigraphically upper part through lower zeolite facies conditions (laumontite-albite-corrensite±chlorite ±smectite±prehnite±pumpellyite; Figures 3(i), 3(j), 4(e), and 4(f)), prehnite-pumpellyite facies conditions (prehnite-pumpellyite-albite±chlorite±laumontite±smectite±corrensite, Figures 3(k) and 4(g)–4(l)), greenschist facies conditions (epidote-albite-chlorite; Figures 3(l), 3(m), 4(m), and 4(n)), and to upper greenschist facies conditions (actinolite-epidote-albite-chlorite; Figures 4(o) and 4(p)) at the base of the sequence at Ely's Peak south of Duluth ([25, 26, 46]; Figure 2). Temperature estimates based on phyllosilicates indicate up to 150°C for smectite-dominant assemblages, 220°C-260°C for corrensite-dominated assemblages, and 275°C for chlorite-dominated ones [27]. At the base of the sequence at Ely's Peak south of Duluth, temperatures during burial are estimated to be between 290°C and 370°C [46]. Variability in the permeability and porosity of the morphological features such as flow bottom, flow top, or massive interior results in different alteration degrees within the sequence [25–27, 45]. In the upper part of the stratigraphic section, massive flow interiors are almost unaltered. Alteration becomes penetrative throughout the flow in the epidote-albite-chlorite assemblage, and massive flow interiors show the same mineralogical features as flow tops or bottoms. Relicts of lower grade may be present occasionally in higher grade metamorphic flows, such as stilbite in laumontite-dominated flows or laumontite in epidote-dominated ones [25, 26]. They are considered as witnesses of the thermal evolution of the sequence. Former vesicles get progressively filled and display specific amygdule mineral sequences mirroring mainly the rise in temperature. Reaction progress as a consequence of temperature and different dissolution rates of the various magmatic constituents leads to the progressive filling of the vesicles [45]. Small-scale hydrothermal systems are responsible for locally increased metamorphic degrees as in the Little Marais area [25] or in the Tofte State Park [45]. A hydrothermal input of seawater is suggested in the greenschist facies basalts based on stable isotope data of

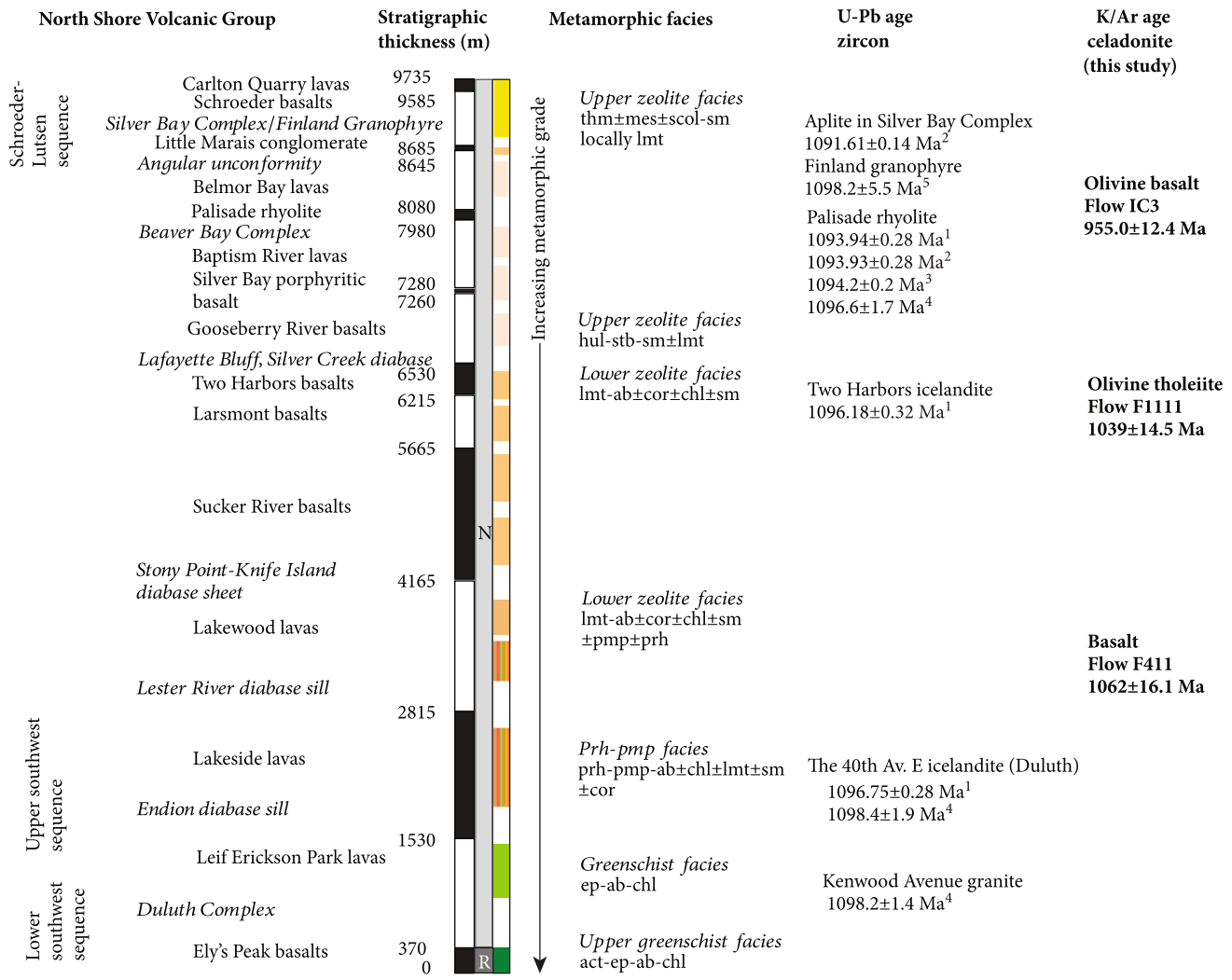

Figure 2: Compilation of stratigraphic information with formational units according to Green et al. [24] with intrusive units in italics, metamorphic facies according to Schmidt [25, 26], Schmidt and Green [92], Schmidt and Robinson [27]; U-Pb data of zircon according to [1]Swanson-Hysell et al. (2019): CAD-ID-TMS $^{238}U/^{206}Pb$, weighted mean; [2]Fairchild et al. (2017): $^{238}U/^{206}Pb$, weighted mean; [3]Schoene et al. (2006): $^{238}U/^{206}Pb$, weighted mean; [4]Davis and Green (1997): $^{207}Pb/^{206}Pb$, weighted mean. [5]Vervoort et al. (2007): U/Pb concordia age. K/Ar ages of celadonite from this study. Mineral abbreviations according to Kretz [93], Whitney and Evans [94]. Dark gray column: reversed geomagnetic polarity; light gray column: normal geomagnetic polarity.

secondary minerals [47]. Using stable oxygen isotope composition in quartz/calcite amygdules, Schmidt and Sharp [48, 49] showed that the fluid developed from a meteoric composition in stratigraphically higher parts to a metamorphic composition controlled by temperature and the breakdown of earlier formed minerals in the stratigraphically lower parts of the sequence. The alteration mode changes in space and time within the sequence and implies the progression of the sequence from a close-to-the-surface alteration mode with input of meteoric water [48, 49], to a burial metamorphic mode and locally to a mode of hydrothermal activity due to continuous magmatism, burial load, and heat transfer from nearby intrusions, such as the Duluth, the Beaver Bay, or the Silver Bay Complexes. Therefore, the term hydrothermal alteration under low-temperature burial conditions is suggested to take into consideration the different alteration environments and the multistage alteration processes controlled mainly by burial depth, rising temperature, and local hydrothermal activity [25, 26, 45].

2.2. Geochronology of Magmatic Sequences in the North Shore Volcanic Group. During the early stage of the Midcontinent Rift magmatism, approximately 1109-1106 Ma [50], the first large basalt flows were deposited on the northeastern flank of the rift. This early stage of magmatism was followed by a period of apparent magmatic quiescence named "latent magmatic stage" and lasted from approximately 1105 to 1100 Ma [50]. The main stage of Midcontinent Rift magmatism occurred from ca. 1100 to 1091 Ma and is characterized by voluminous, normally polarized basalts of the NSVG ([33, 34, 37, 51, 52]; Figure 2).

FIGURE 3: Morphological features of North Shore Volcanics: (a) flow contact with massive flow interior to the right and flow top of older flow to the left; (b) Pahoehoe lava; (c) interlayered terrestrial sediments deposited by braided streams; (d) amygdaloidal flow top with scolecite; (e) amygdaloidal flow top with mainly calcite and saponite, as well as a horizontal zone with heulandite (orange-red); (f) pipe amygdule zone at base of lava flow with saponite and calcite. The direct contact to the older flow is evident by the red oxidation color of the base of the younger flow; (g–i) characteristic zeolites: (g) fibrous stilbite, (h) heulandite, and (i) laumontite; (j) laumontite with corrensite/smectite (light green), chlorite (dark green), and celadonite (blue-green); (k) amygdule with light green prehnite and native copper; (l) amygdaloidal flow top with epidote-albite-chlorite assemblage; (m) dark green Fe-rich chlorite; (n) massive flow interior with light green saponite. Red tip of match is 3 mm long. The coin in (g, i, j, m) has a diameter of 0.75 inches or 19.05 mm, and the half dollar in (k) has a diameter of 1.2 inches or 30.21 mm. The pocketknife is 8.5 cm long; hammer length is 28 cm.

In the southwestern limb of the NSVG near Duluth, the Kenwood Avenue granite intrudes the Leif Erickson lavas and is considered to be one of the youngest phases related to the Duluth Complex (Figure 2). It was dated at 1098.2 ± 1.4 Ma ($^{207}Pb/^{206}Pb$, weighted mean, [37]). The main stage of magmatism (Figure 2) is represented by the icelandite exposed along the 40th Ave E in Duluth and is dated at 1096.75 ± 0.28 Ma (CA-ID-TIMS $^{206}Pb/^{238}U$ age; [34]) and 1098.4 ± 1.9 Ma ($^{207}Pb/^{206}Pb$, weighted mean, [37]). The Two Harbors icelandite gives a CA-ID-TIMS $^{206}Pb/^{238}U$ age of 1096.18 ± 0.32 Ma [34]. The Palisade Rhyolite (Figure 2) displays a CA-ID-TIMS $^{206}Pb/^{238}U$ age of 1093.94 ± 0.28 Ma [34] dated formerly by Davis and Green [37] at 1096.6 ± 1.7 Ma ($^{207}Pb/^{206}Pb$, weighted mean), and the Finland granophyre (Figure 2) is dated at 1098.2 ± 5.5 Ma ([52]; $^{207}Pb/^{206}Pb$, weighted mean). The currently youngest age in the NSVG was determined in the aplite of the Silver Bay Complex [34] yielding an age of 1091.61 ± 0.14 Ma (CA-ID-TIMS $^{206}Pb/^{238}U$ age).

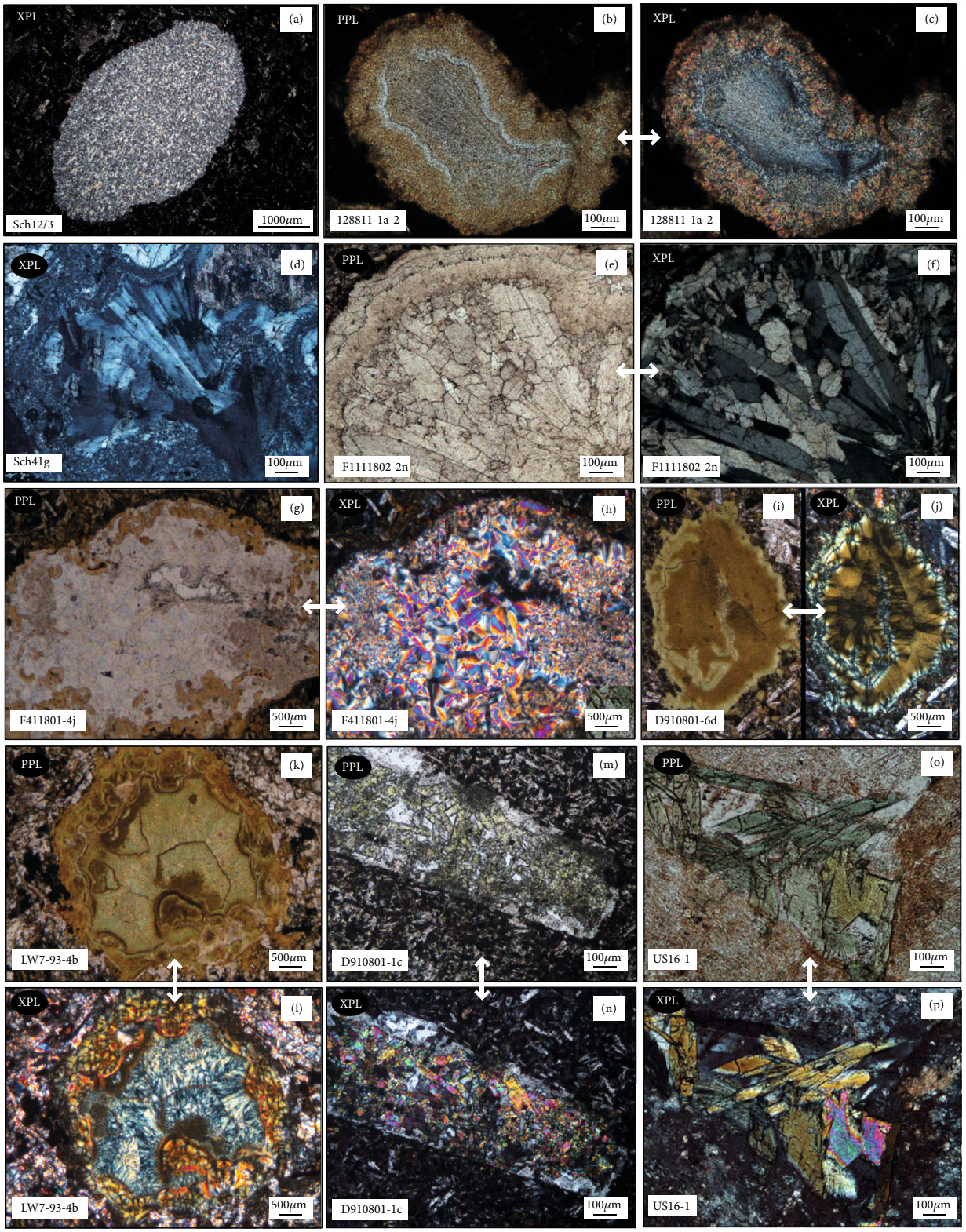

Figure 4: Petrography of altered North Shore Volcanics: (a) amygdule with thomsonite from thomsonite±mesolite±-scolecite-smectite zone; (b, c) mordenite at rim followed by scolecite from thomsonite±mesolite±-scolecite-smectite zone; (d) amygdule with stilbite from heulandite-stilbite-smectite zone; (e, f) amygdule with laumontite showing the increase of size of laumontite crystals from rim to center; (g–l) laumontite-albite-corrensite±chlorite±smectite±prehnite±pumpellyite zone; (g, h) amygdule with prehnite; (i, j) light green smectite at rim of amygdule followed by corrensite; (k, l) amygdule of pumpellyite; (m, n) epidotisation of magmatic Ca-rich plagioclase from epidote-albite-chlorite zone; (o, p) actinolite-epidote in amygdule from actinolite-epidote-albite-chlorite zone. PPL = plane-polarized light; XPL = cross-polarized light.

Table 1: Lava flows with dated celadonite, their geographic coordinates, topographic quadrangle, lithological unit, metamorphic zone, and metamorphic mineral assemblages according to Schmidt [25, 26]. Estimation of total thickness (9735 m), stratigraphic position of flow and lithological unit according to Green et al. [24]. Mineral abbreviations according to Kretz [93], Whitney and Evans [94].

Lava flow	Geographic coordinates	Topographic quadrangle	Lithological unit	Metamorphic zone with assemblage	Depth (m)
IC3: Olivine basalt	47°20′54″N 091°10′52″W	Illgen City	Belmore Bay lavas	Upper zeolite facies hul-stb-sm	ca. 8300
F1111: Olivine tholeiite	47°01′39″N 091°38′12″W	Two Harbors	Two Harbors basalts	Lower zeolite facies lmt-ab-cor±chl±sm±prh±pmp	ca. 6350
F41: Basalt	46°53′23″N 091°54′26″W	French River	Lakewood lavas	Lower zeolite facies lmt-ab-cor±chl±sm±prh±pmp	ca. 3600

3. Sampling, Materials and Methods

3.1. Sampling and Characterization of Celadonite. Celadonite occurrences were identified in three flows (basalt F411, olivine tholeiite F1111, and olivine basalt IC3) and provided sufficient material to be characterized and dated. Their location, geographic coordinates, and metamorphic facies are indicated in Figures 1 and 2 and Table 1. Polished thin sections of celadonite-bearing amygdaloidal units were examined with the polarized light microscope, and the SEM imaging was performed at the University of Geneva using a JEOL JSM7001F scanning electron microscope equipped with the energy-dispersive X-ray spectroscopy system JED 2300.

3.2. Electron Microprobe Analysis. The chemical composition of celadonite was obtained by using a JEOL JXA-8200 microprobe at the University of Geneva. The accelerating voltage was set at 15 kV, beam current was 10 nA, and beam diameter was 1 μm. Peak counting times were between 10 s and 20 s, and background counting times were between 15 s and 20 s. The microprobe is equipped with five automated wavelength-dispersive spectrometers (LIF, PET, TAP, LDE1, and LDE2). The element abundances were determined relative to the standards: forsterite (Mg), wollastonite (Si, Ca), fayalite (Fe), orthoclase (K, Al), $MnTiO_3$ (Mn, Ti), and jadeite (Na). Raw data were reduced with the PAP routine. In a routine microprobe analysis, the error is generally <1% with errors increasing for low concentrations of an element, if the totals are correct and the stoichiometry of the mineral is respected. Since celadonite contains Fe^{2+}, Fe^{3+}, and OH groups which were not determined, the resulting sums are always below 100%.

3.3. K/Ar Age Determination. Ages of celadonite were obtained from three lava flows using the K/Ar method [53]. The K-Ar dating was carried out at the University of Göttingen (Germany), and details of argon and potassium analyses are given in Wemmer [54]. Celadonite was extracted from individual amygdules of each flow and gently crushed by hand using a mortar and pestle. K_2O was determined using a BWB XP flame photometer. Celadonite powders were dissolved in a mixture of HF and HNO_3. The pooled error of the duplicate potassium determinations in samples and standards is better than 0.8%. The samples were preheated to 120°C at high vacuum for at least 24 h to reduce the amount of atmospheric argon attached to the mineral surfaces. The sample was dropped into a molybdenum crucible under vacuum and heated by induction for 30 min, increasing the temperature to nearly 2.000°C. The argon isotopic composition was analyzed in a Pyrex glass extraction and purification line coupled to an ARGUS VI multicollector mass spectrometer operating in a static mode. The amount of radiogenic ^{40}Ar was determined by the isotope dilution method using a highly enriched ^{38}Ar spike, which was calibrated against the international biotite standard HD-B1 (24.18 ± 0.09 Ma) introduced by Fuhrmann et al. [55] and reevaluated by Schwarz and Trieloff [56]. All three samples were measured in a batch of 28 unknown samples and 4 HD-B1 standards which yielded deviations of 0.23%, 0.55%, 0.58%, and 0.26%. The extracted gases were purified in a multistage process by Ti- and SORB-ACs getters. The reproducibility of the Ar isotopic results was controlled by repetitive analysis of the Standard HD-B1. The K/Ar ages were calculated with the usual decay constants [57], and the overall error is <1% (2σ).

3.4. X-Ray Diffraction. X-ray diffraction was done at the University of Geneva using a PANanalytical Empyrean diffractometer. Measurements were carried out in air-dried conditions in the Bragg-Brentano geometry using CuKα radiation (1.54060 Å), 45 keV and 40 mA, and were scanned from 3° to 70° 2θ. In addition, X-ray powder diffraction data were also collected at the Swiss Norwegian Beamlines of ESRF (European Synchrotron Radiation Facility, Grenoble, France) at room temperature. The samples were sealed into borosilicate capillaries of 0.5 mm diameter which were spun during data acquisition. The data were recorded on the Dectris Pilatus M2 detector at a wavelength of 0.7980 Å calibrated with NIST SRM640c Si standard.

4. Results

4.1. Occurrence and Petrographic Description of Celadonite. Celadonite was observed in three lava flows within different stratigraphic horizons of the NSVG (Figures 1 and 2, Table 1). Celadonite is absent in the highly amygdaloidal flow top units and occurs in isolated amygdaloidal units in the more massive parts (Figures 3(j), 5(a), and 5(b)). This is in agreement with Gallahan and Duncan [15] who also report

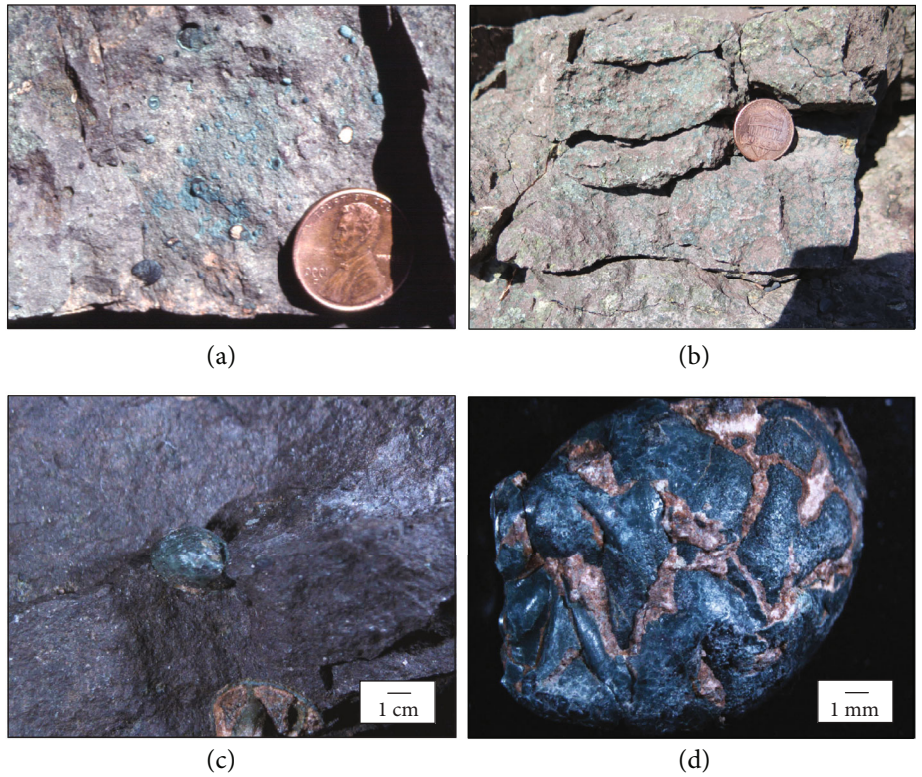

Figure 5: Typical outcrop occurrence of celadonite: (a) occurrence of celadonite in amygdules of the massive part of flow IC3 (Illgen City Quadrangle); (b) localized occurrence of celadonite in amygdules of the massive part of flow F411 (French River Quadrangle); (c) individual celadonite in amygdule of massive flow unit; (d) individual celadonite amygdule with quartz separated from amygdule and used for age dating. The coin in (a, b) has a diameter of 0.75 inches or 19.05 mm.

higher abundance of celadonite in areas of massif flow units. Celadonite can be easily sampled from individual amygdules (Figures 5(c) and 5(d)). The stratigraphically lowermost flow F411 (Figures 1 and 2) occurs within the lithostratigraphic unit named the Lakewood lavas [24]. Flow F1111 (Figures 1 and 2) is located in the lithostratigraphic unit named the Two Harbors basalts [24] and is described in detail in Schmidt [25, 26] and Schmidt and Robinson [27]. Both flows, F411 and F1111, occur in the lower zeolite facies characterized by the occurrence of the mineral assemblage laumontite-albite-corrensite±chlorite±smectite±prehnite ±pumpellyite. Flow IC3 belongs to the Belmore Bay lavas [24], and the metamorphic assemblage shows upper zeolite facies conditions characterized by the assemblage heulandite-stilbite-smectite [25, 26]. Celadonite is recognized in thin sections by its intensive bluish-green color, its anomalous blue-green interference colors, and its needle-like habit (Figure 6). It occurs interstitially (Figure 6(a)) and replaces magmatic olivine. It is dominant in amygdules where it crystallizes after an Fe-oxide/hydroxide rim at the wall of the amygdule (Figures 6(b) and 6(c)) or directly on the vesicle wall (Figures 6(d)–6(f)), after chalcedony (Figures 6(g) and 6(h)) or after saponite (Figures 6(j) and 6(k)). Crystals of celadonite radiate also from Fe-oxide (Figure 6(i)). A BSE image of an amygdule with celadonite at the rim and chlorite in the center documents the rise in temperature during infilling of the amygdule (Figure 6(l)).

4.2. Microprobe Analysis. Because of coupled substitution and charge balancing constraints between celadonite $K_2Mg_2Fe_2^{+3}Si_8O_{20}(OH)_4$, ferroceladonite $K_2Fe_2^{2+}Fe_2^{3+}Si_8O_{20}(OH)_4$, and ferroaluminoceladonite $K_2Fe_2^{2+}Al_2Si_8O_{20}(OH)_4$, the binary diagram $4M^+/Si$ versus $Fe^T/\sum$ octahedral is used to show the observed compositional range of celadonite (Figure 7). A selection of microprobe analyses is listed in Table 2. The contents of Fe^{2+} and Fe^{3+} were not determined. Since all iron is given as Fe^{2+} and OH content is not known, the resulting sums are below 100%. Low totals are commonly reported for microprobe analysis (e.g., [15, 18, 58]). The term celadonite is used for all compositions rather than being further subdivided because all flows show variable Al-Fe composition. The NSVG celadonites show quite a compositional range in Fe-Al composition, and every celadonite occurrence displays its own characteristic compositional field (Figure 7). The stratigraphically lower flows, F1111 and F411, yield higher $Fe^T/\sum$ octahedral cations due to their higher Fe^T octahedral content (Table 2, Figure 7). Si varies between 7.883 and 7.507 a.p.f.u. (22 oxygens). The octahedral sum yields values below 4 a.p.f.u. (22 oxygens) for stratigraphically lower flows typical for dioctahedral mica and values around 4 for the stratigraphically higher flow IC3 (Table 2). The interlayer site occupancy is <2 a.p.f.u. with mainly K and minor Ca and Na contents and is generally lower for IC3 (1.338-1.898, a.p.f.u., 22 oxygens) than for the flows F1111 and F411 (1.61-1.839 a.p.f.u., 22 oxygens). The studied

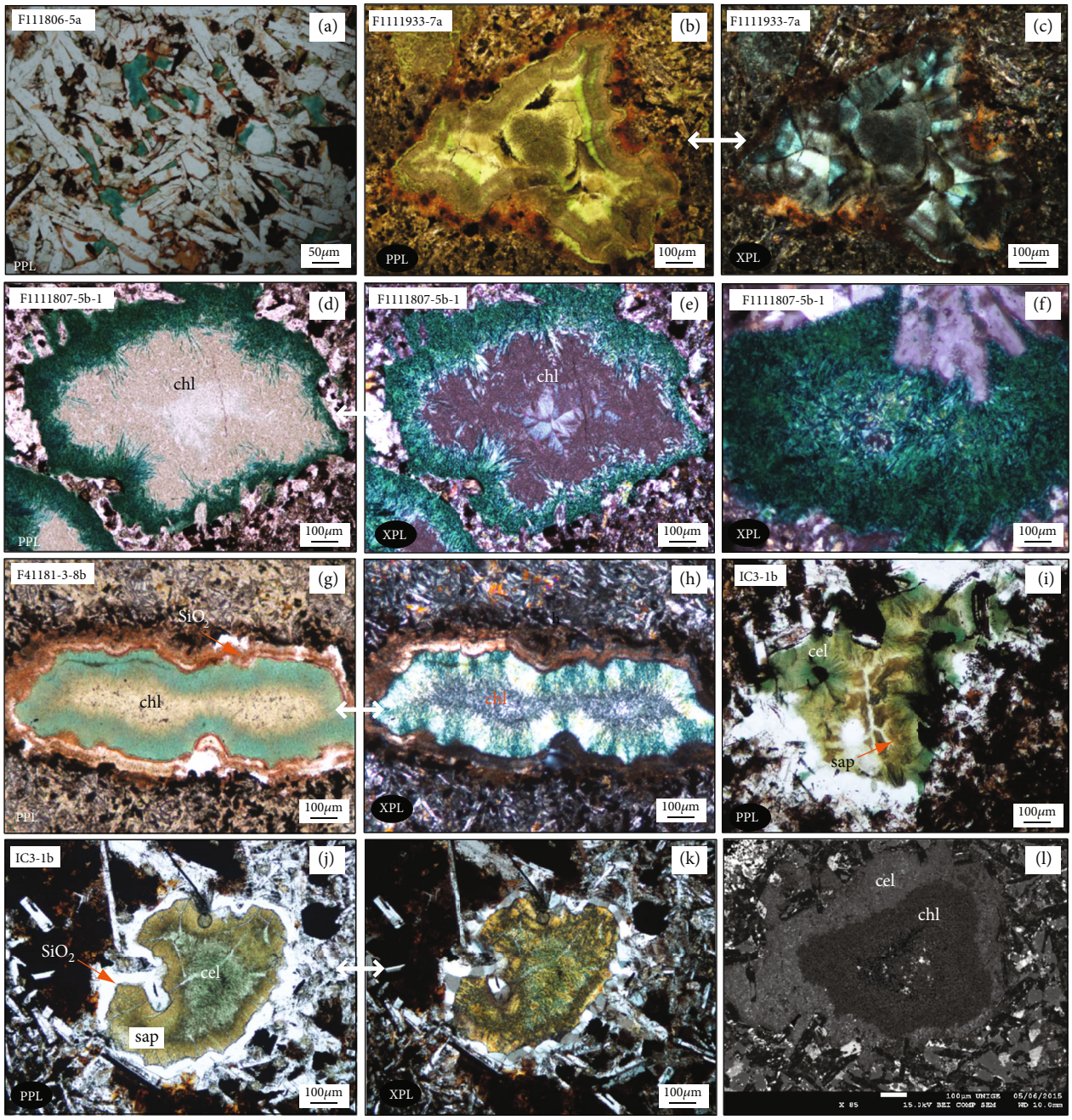

Figure 6: Microscopic images of blue-green celadonite; (a) celadonite as interstitial phase; (b, c) celadonite crystallizes in amygdule after Fe-oxide formation; (d, e) fibrous celadonite crystallizes directly at the amygdule wall followed by chlorite indicating a rise in temperature; (f) fibrous celadonite at the rim of amygdule; (g, h) fibrous celadonite crystallizes after rim of chalcedony; (i) celadonite starting to crystallize around hematite with saponite (sap); (j, k) celadonite crystallizes after saponite; (l) BSE image of amygdule mineral sequence of celadonite at rim followed by chlorite.

celadonites (Figure 7) are compared with the compositional celadonite fields from the continental flood basalts of the Columbia River Basalts Group [19], from the oceanic Troodos ophiolite [15], and from the oceanic crust [14]. Individual analyses from New Zealand by Li et al. [59], the Twin Creek in Wyoming, and the Krivoi Mining District in Russia by Drits et al. [58] are plotted as well (Figure 7). The composition of the stratigraphically upper flow IC3 plots towards the saponite field and celadonite is intergrown with saponite as also evidenced by the XRD data (Figure 8(a)). Flow F1111 displays also Al-Fe variation and F411 plots in the compositional field of Humphris [14] overlapping with the compositional field of Gallahan and Duncan [15].

4.3. XRD Data. XRD analysis of the bluish-green mineral phase from the vesicles of the three analyzed flows (Figure 8 and Table 3) is consistent with celadonite as the

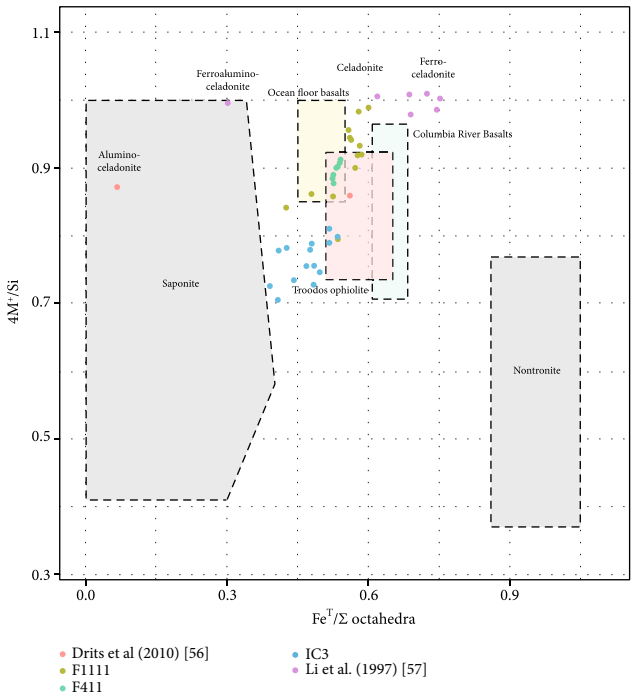

FIGURE 7: $4M^+$/Si versus FeT/octahedra in flows F411, F1111, and IC3, as well as values from the literature. A compositional range between more Al-rich and more Fe-rich compositions is observed. The stratigraphically upper flow trends to more Al-rich compositions, while the stratigraphically lower ones yield more Fe-rich compositions. Field of ocean floor basalts according to Humphris et al. [14], Columbia River Basalts according to Baker et al. [19] and Troodos ophiolite according to Gallahan and Duncan [15] $M^+ = 2Ca + Na + K$.

dominant phase [19, 58, 60–64]. Table 3 lists the corresponding peaks measured with synchrotron radiation ($\lambda = 0.798\,Å$) and CuKα radiation ($\lambda = 1.54060\,Å$) and d-spacing and intensities used for identification. The d-spacings of celadonite coincide particularly well with the values reported by Wise and Eugster [63] (PDF 00-017-0521). Celadonite from the stratigraphically upper flow IC3 shows the (060) peak characteristic of a dioctahedral mica at 1.510 Å. The (002) peak is obscured by destructive interference as also known from other Fe-rich micas. According to Wise and Eugster [63], the peaks at 3.633 Å and 3.088 Å correspond to $\bar{1}12$ and 112 (Table 3), respectively, and are characteristic for the 1 M polymorph. Peaks with d-spacings of 3.50 Å and 3.12 Å corresponding to $11\bar{4}$ and 114 would be indicative of a 2 M polymorph, but these values are not observed. Celadonite from sample IC3 is intergrown with saponite and hematite (Figure 8(a)). The Rietveld quantification yields 83% celadonite, 16% saponite, and 1% hematite. Rietveld quantification of a sample of flow F1111 yields 33% chlorite, 63% celadonite (partly interstratified with smectite), 3% quartz, and traces of hematite (<1%). Celadonite of flow F1111 (Figure 8(b)) shows similar d-spacings as sample IC3, and the (060) spacing is present at 1.510 Å (Table 3). Note that the peak at 9.95 Å shows an asymmetric peak towards lower angles indicating smectite interlayering. In addition, a textured sample was prepared of F1111 (Figure 8(c)). It shows the *00l* d-spacings for celadonite and minor chlorite (Table 3). A double peak at 10.048 Å and 9.977 Å is present, probably reflecting slightly different compositions as shown by the microprobe analysis. The values coincide well with the values of celadonite as reported by Zhukhlistov et al. [65] (PDF 01-083-2008) and Slovenec et al. [62] (PDF 00-0050-1580). Since it is a textured sample, the (060) peak is not recorded. Peak decomposition obtained from another sample of the same flow using NEWMOD® [66] reveals mainly celadonite with minor chlorite, chlorite/smectite, and laumontite (Figure 8(d)) as evidenced also in Figure 8(b) by the asymmetric peak and a shift towards more saponitic compositions as also observed from microprobe analysis (Figure 7).

4.4. K/Ar Ages. The K/Ar ages range between 1062.6 ± 16 Ma (sample F411) and 955.0 ± 12 Ma (IC3) and become younger within the stratigraphic section (Table 4, Figure 2). They are reliable measurements of celadonite crystallization and fit in the known geochronological pattern. The low-temperature formation, the fibrous habit of celadonite, and the long-lasting alteration process might imply thermally controlled loss of radiogenic $^{40}Ar*$. This should result in younger ages of celadonite in stratigraphically lower flows; however, older ages are observed, and the ages get younger towards the stratigraphic top. Nevertheless, as basic parameters for celadonite dating like closure temperature and retentivity are not known, a loss of $^{40}Ar*$ cannot be ruled out entirely.

The stratigraphically oldest flow gives the oldest age (1062 ± 16 Ma, sample F411; Table 2, Figure 2), the sample F1111 yields an intermediate age of 1039.4 ± 14 Ma (Table 2, Figure 2), and the youngest flow IC3 is dated at 955.0 ± 12 Ma (Table 2, Figure 2).

The age dates and stratigraphic positions of the flows (Table 1) within the NSVG also allow for a first estimation of the burial rate in the NSVG. By using the oldest and the youngest ages of flows F411I and IC3, respectively, and a stratigraphic difference of 4700 m, a burial rate of 0.04 km.Ma^{-1} can be calculated. By using the celadonite age dates of F411 and F1111 and a stratigraphic difference of 2750 m, a burial rate of 0.11 km·Ma^{-1} is determined. A burial rate of 0.11 km·Ma^{-1} is also determined by using the youngest zircon age of the aplite in the Silver Bay complex (1091 Ma) considered being the best maximum age constrained for the Schroeder-Lutsen basalts [33], the oldest celadonite age date of F411 (1062.6 Ma), and a difference in stratigraphic thickness of 5400 m. The determined burial rates are lower than the burial rates in convergent settings, i.e., in the Grenville orogeny of North America which are calculated to be at 0.63 ± 0.1 km·Ma^{-1} [67] and support the long-lasting alteration processes.

5. Discussion

The three K/Ar ages of celadonite give a postdepositional thermal window of 107 myrs. Hydrothermal alteration linked to hydrothermal intrusive events normally occurs during

Table 2: Selected microprobe data of celadonite from flows F1111, F411, and IC3 based on 22 oxygens. $M^+ = 2Ca+Na+K$.

	F1111	F1111	F1111	F1111	F1111	F1111	F1111	F411	F411	F411	IC3-1	IC3-1	IC3-1	IC3-1	IC3-1	IC3-1
SiO_2	55.68	53.96	55.24	54.16	54.00	56.84	54.74	53.27	54.77	54.32	50.75	53.93	53.81	53.67	53.55	52.66
TiO_2	0.00	0.00	0.02	0.02	0.10	0.03	0.24	0.00	0.00	0.00	0.06	0.05	0.04	0.05	0.08	0.17
Al_2O_3	8.40	4.20	2.25	5.32	3.10	2.56	3.40	3.91	2.70	2.90	6.80	8.47	7.58	5.72	6.46	1.76
FeO	18.31	21.6	22.53	22.8	20.27	21.73	21.11	21.43	21.65	18.76	18.92	17.29	18.29	20.13	19.34	21.59
MnO	0.06	0.12	0.09	0.13	0.17	0.00	0.03	0.03	0.00	0.00	0.05	0.05	0.04	0.00	0.04	0.00
Mgo	5.12	5.34	5.90	5.62	5.78	5.78	6.19	5.42	6.03	6.06	5.62	6.51	5.71	5.23	5.37	5.02
CaO	0.55	0.11	0.03	0.18	0.22	0.18	0.30	0.09	0.05	0.07	0.50	0.61	0.50	0.37	0.49	0.30
Na_2O	0.03	0.20	0.09	0.11	0.00	0.08	0.10	0.02	0.02	0.00	0.06	0.08	0.14	0.14	0.13	0.24
K_2O	8.85	9.70	10.41	9.41	9.94	9.84	9.58	9.39	9.64	9.54	7.30	6.97	7.44	7.75	7.55	9.32
P_2O_5	0.02	0.04	0.00	0.05	0.05	0.02	0.02	0.00	0.00	0.00	0.00	0.00	0.00	0.00	0.00	0.02
Formular																
Si	7.507	7.557	7.673	7.384	7.689	7.781	7.614	7.718	7.826	7.804	7.394	7.438	7.493	7.566	7.532	7.883
Al tetrahedral	0.493	0.443	0.327	0.616	0.311	0.219	0.386	0.282	0.174	0.196	0.606	0.562	0.507	0.434	0.468	0.117
∑ tetrahedral	8.000	8.000	8.000	8.000	8.000	8.000	8.000	8.000	8.000	8.000	8.000	8.000	8.000	8.000	8.000	8.000
Al octahedral	0.842	0.250	0.041	0.239	0.209	0.194	0.172	0.385	0.281	0.295	0.561	0.814	0.737	0.517	0.603	0.193
Al total	1.335	0.693	0.368	0.855	0.520	0.413	0.557	0.668	0.455	0.491	1.168	1.377	1.244	0.950	1.071	0.311
Fe^T	2.065	2.530	2.617	2.609	2.414	2.488	2.456	2.336	2.328	2.314	2.305	1.994	2.130	2.373	2.275	2.421
Mn	0.007	0.014	0.011	0.015	0.021	0.000	0.004	0.003	0.000	0.000	0.006	0.005	0.004	0.000	0.005	0.000
Mg	1.029	1.115	1.222	1.142	1.227	1.180	1.284	1.171	1.285	1.298	1.221	1.339	1.185	1.099	1.126	1.120
Ti	0.000	0.000	0.002	0.002	0.011	0.003	0.025	0.000	0.000	0.000	0.007	0.005	0.004	0.005	0.008	0.019
Ca	0.079	0.017	0.004	0.026	0.034	0.026	0.045	0.015	0.007	0.011	0.077	0.091	0.075	0.056	0.073	0.048
Na	0.008	0.054	0.024	0.029	0.000	0.021	0.027	0.005	0.006	0.000	0.016	0.021	0.038	0.039	0.036	0.070
K	1.522	1.733	1.845	1.637	1.806	1.718	1.700	1.735	1.757	1.749	1.357	1.226	1.322	1.394	1.355	1.780
P	0.002	0.005	0.000	0.006	0.006	0.002	0.002	0.000	0.000	0.000	0.000	0.000	0.000	0.000	0.000	0.003
∑K+Ca+Na	1.610	1.804	1.873	1.692	1.839	1.766	1.772	1.755	1.770	1.760	1.450	1.338	1.435	1.488	1.464	1.898
∑octahedral	3.943	3.909	3.893	4.008	3.882	3.864	3.940	3.896	3.894	3.907	4.100	4.157	4.061	3.995	4.018	3.754
∑12 cation	11.94	11.91	11.89	12.01	11.88	11.86	11.94	11.90	11.89	11.91	12.10	12.16	12.06	11.99	12.02	11.75
Fe^T/∑octahedral	0.524	0.647	0.672	0.651	0.622	0.644	0.623	0.600	0.598	0.592	0.562	0.480	0.525	0.594	0.566	0.645
$4M^+$/Si	0.938	0.945	0.959	0.923	0.961	0.973	0.952	0.965	0.978	0.976	0.924	0.930	0.937	0.946	0.942	0.985

relatively short time intervals < 1 myrs. For example, Naranjo et al. [68] report a time interval of 1.1 myrs for the entire intrusive and hydrothermal mineralization events at the La Colosa Porphyry system, and Henry et al. [69] report a brief duration of no more than 0.1 myrs for the hydrothermal activity at Round Mountain as determined by $^{40}Ar/^{39}Ar$ ages of adularia. Hur et al. [70] report K/Ar ages of an argillitic alteration in andesite on King George Island in Antarctica being 10 myrs younger than the adjacent alteration. The here reported long and probably discontinuous duration of the beginning alteration is therefore not related to hydrothermal intrusive activity, but to the onset of the beginning burial metamorphism at shallow depths (<500 m) after the deposition of the NSVG. Although the age span of later alteration events following celadonite crystallization and linked to the crystallization of the zeolite, epidote, or actinolite assemblages has not been determined, they are supposed to have occurred within this time window.

5.1. Formation of Celadonite. The formation temperature of celadonite is typically considered to be between 25°C and 60°C under oxidizing alteration conditions in oceanic basalts (e.g., [71]) and generally linked to a marine environment. Based on paragenetic textures, Rodriguez-Losada et al. [72] suggest a formation temperature of approx. 90°C for celadonite in the Punta Payata basalts on the Canary Islands. In DSDP/ODP hole 504B of the oceanic crust of the eastern Pacific, celadonite is present up to a depth of approx. 550 m together with saponite [73]. In the continental flood basalts of the Miocene Grande Ronde Basalts of the Columbia River Basalt Group in Washington, celadonite was formed slowly at temperatures between 15 and 35°C, an oxygen fugacity buffered by interaction with basalt and the Grande Ronde Aquifer [19]. Exploratory experiments by Velde [74] at 400°C and 4.5 kb and by Wise & Eugster [63] at 410°C suggest Mg-Fe celadonite to be stable comprising the diagenetic and low-grade metamorphic stability fields. Ferroceladonite was also shown by Miller et al. [75] to form in two weeks from nontronite in a simulated burial diagenetic system at temperatures between 250°C and 300°C. Celadonite precipitation is locally controlled, and different mechanisms are suggested for celadonite formation. As shown in thin section images

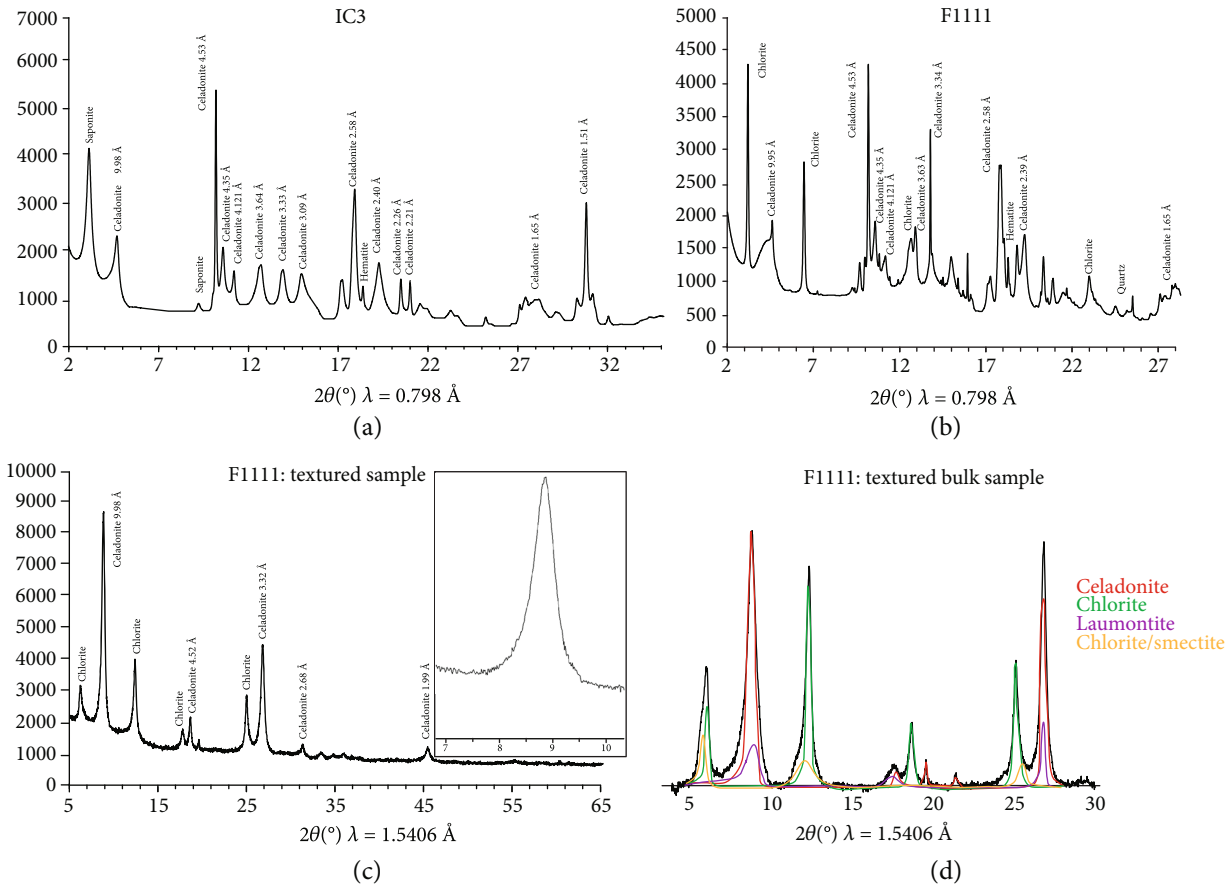

FIGURE 8: XRD pattern of various bulk amygdule contents of celadonite; (a) celadonite from flow IC3 intergrown with saponite (wavelength 0.7980 Å); (b) celadonite from flow F1111 intergrown with chlorite (wavelength 0.7980 Å); (c) celadonite from flow F1111 with two maxima at 8.793 and 8.862 ($2\theta^{\circ}$ CuKα); (d) peak decomposition using NEWMOD of mineral phases in an amygdule of flow F1111 ($2\theta^{\circ}$ CuKα) showing dominant celadonite and minor amounts of facies characteristic minerals such as chlorite and laumontite.

(Figure 6), celadonite occurs interstitially intergrown to plagioclase, olivine and clinopyroxene (Figures 6(a)), crystallizes after an Fe-oxide/hydroxide rim at an amygdule (Figure 6(b) and 6(c)), directly on the vesicle wall (Figures 6(d)–6(f)), after chalcedony (Figures 6(g) and 6(h)) or after saponite (Figures 6(i)–6(k)). Chlorite often crystallizes after celadonite (Figure 6(l)). Celadonite precipitation probably proceeded via progressive dissolution and precipitation of saponite to celadonite [76] or directly from oxidizing to reducing conditions [13]. The celadonite-saponite assemblage in flow IC3 points to a crystallization starting with saponite/celadonite in close-to-surface oxidizing conditions and input of meteoric water (Figure 6(i)). Stable isotope composition of smectite and quartz and calcite in stratigraphically upper flows suggests that meteoric water was dominant in the higher portions of the sequence [47–49]. Celadonite lining up the vesicle rims was succeeded by mineral assemblages which reflect rising temperatures during burial and changed conditions related to hydrothermal activity during the burial process. Lower zeolite facies conditions were established in flows F1111 and F411 suggesting that celadonite is stable under these conditions. It might have crystallized under similar conditions as in flow IC3. Celadonite is not found in the epidote-albite-chlorite or actinolite-epidote-albite-chlorite assemblages. The observed occurrences of celadonite in the NSVG would indicate a lower temperature stability of <100°C and an upper thermal stability of approximately 250°C, with formation in a nonmarine environment with meteoric water as also observed by Baker et al. [19] for the Columbia River Basalts. A possible source for K is either volcanic glass or magmatic plagioclase which shows up to 6 Mol % Or and alters to albitic compositions [25, 26].

Celadonite is a relic low-temperature mineral and might have been more widespread at the beginning of alteration but was replaced by other phases during the ongoing alteration which might explain its occurrence in massive flow interiors. Celadonite crystallization was followed during a later alteration phase by the heulandite-stilbite-smectite assemblages in the stratigraphically upper flow or by the laumontite-albite-corrensite±chlorite±smectite±prehnite ±pumpellyite assemblage in the stratigraphically lower flows clearly indicating a rise in temperature and an ongoing polyphase posteruptive thermal history [25–27].

The three K/Ar dates of celadonite between 1062 ± 16 Ma and 955 ± 12 Ma are interpreted as crystallization ages. The ages get younger from the stratigraphically lower flows to

Table 3: X-ray data of celadonite and other phases as determined by synchrotron radiation using $\lambda = 0.798$ Å. Peak positions for CuKα were calculated, are marked with $*$ and are listed for comparison. Conventional analysis using CuKα $\lambda = 1.54060$ is also given.

IC3 Celadonite PDF 00-017-0521				F1111 Celadonite PDF 00-017-0521					F1111 textured sample Celadonite (PDF 01-083-2008)				Saponite (PDF 00-030-0789)				Chlorite (00-024-0506)			
$\lambda = 0.798$ Å Pos. (°2Th.) Measured	$\lambda = 1.54060$ Å *Pos. (°2Th.) Calculated	d-spacing (Å)	Rel. Int (%)	$\lambda = 0.798$ Å Pos. (°2Th.)* Measured	$\lambda = 1.54060$ Å *Pos. (°2Th.) Calculated	d-spacing (Å)	Rel. Int (%)	hkl	$\lambda = 1.54060$ Å Pos. (°2Th.) Measured	d-spacing (Å)	Rel. Int. Int. (%)	hkl	$\lambda = 0.798$ Å Pos. (°2Th.) Measured	$\lambda = 1.54060$ Å *Pos. (°2Th.) Calculated	d-spacing (Å)	Rel. Int (%)	$\lambda = 0.798$ Å Pos. (°2Th.) Measured	2θ $\lambda = 1.54060$ Å *Pos. (°2Th.) Calculated	d-spacing (Å)	Rel. Int (%)
4.585	8.854	9.975	25.7	4.595	8.877	9.953	17.8	001	8.793	10.048	93.1	001	3.080	5.949	14.845	55.0	3.196	6.172	14.307	61.4
10.110	19.581	4.528	100.0	10.113	19.594	4.527	67.2	020	8.862	9.971	100.0	001	9.169	17.754	4.992	3.8	6.409	12.390	7.138	40.0
10.514	20.368	4.355	26.5	10.516	20.381	4.354	18.7	$\bar{1}11$	17.786	4.983	8.3	002	10.062	19.494	4.550	100.0	9.611	18.615	4.763	8.3
11.104	21.521	4.124	15.5	11.112	21.546	4.121	8.3	021	19.632	4.518	4.3	020	26.910	53.385	1.715	7.1	9.893	19.164	4.628	8.2
12.602	24.456	3.635	16.6	12.610	24.480	3.633	12.8	$\bar{1}12$	26.793	3.325	49.0	003	Hematite (PDF 072-469)				12.824	24.901	3.573	16.5
13.661	26.538	3.355	13.7	13.702	26.629	3.345	47.0	022	33.436	2.678	3.0	023	18.232	35.622	2.518	11.0	17.186	33.531	2.670	8.2
13.785	26.782	3.325	15.2					003	35.995	2.493	1.9	004	25.027	49.454	1.842	4.1	17.987	35.130	2.552	17.4
14.832	28.848	3.091	14.6	14.849	28.892	3.088	9.9	112	45.513	1.991	6.0	005	27.222	54.041	1.696	9.0	18.744	36.648	2.450	16.0
16.994	33.136	2.700	14.1	15.269	29.724	3.003	4.6	004	55.346	1.659	1.0	006	28.937	57.679	1.597	3.5	20.300	39.781	2.264	14.7
17.128	33.402	2.679	15.1	17.186	33.531	2.670	8.2	023	65.553	1.423	1.0	007	30.093	60.157	1.537	9.8	22.885	45.040	2.011	9.5
17.646	34.436	2.601	34.7	17.680	34.517	2.596	39.6	130					31.010	62.141	1.493	12.8	26.903	53.372	1.715	5.2
17.791	34.725	2.580	55.0	17.808	34.774	2.578	39.0	$\bar{1}31$					31.857	63.987	1.454	4.0	29.957	59.864	1.544	28.0
19.122	37.391	2.402	21.6	19.210	37.583	2.391	19.9	$\bar{1}32$					34.542	34.972	1.344	0.7				
20.303	39.770	2.264	14.8	20.300	39.781	2.264	14.7	040												
20.822	40.819	2.208	14.0	20.832	40.857	2.207	7.5	041												
21.381	41.953	2.151	5.1					$\bar{1}33$												
28.043	55.754	1.647	8.2	27.992	55.668	1.650	5.4	$\bar{1}52$												
30.643	30.646	1.510	53.6	30.638	61.333	1.510	41.7	060												

Table 4: K/Ar age results of the dated celadonite. STP: standard temperature pressure.

Sample	K_2O (Wt. %)	$^{40}Ar*$ (nl/g) STP	$^{40}Ar*$ (%)	Age (Ma)	2σ-error (Ma)	2σ-error (%)
IC3	4.39	178.36	98.98	955.0	12.4	1.3
F1111	5.62	254.64	98.98	1039.4	14.5	1.4
F411	4.87	227.47	97.75	1062.6	16.1	1.5

the stratigraphically upper flows. In the stratigraphically older lava flows, crystallization of celadonite occurred locally after the eruption and the flows were consequently buried by further eruption events under lower zeolite facies metamorphism. The stratigraphically upper flow was deposited later and therefore yields a younger celadonite crystallization age. The age span over which celadonite crystallization took place lasted more than 100 myrs and suggests a long duration of posteruptive thermal history in a thick basaltic sequence. Celadonite crystallized during surface fluid-rock interaction in an oxidizing environment affecting the rocks only locally. The posteruptive thermal history that started with celadonite crystallization was followed by burial resulting in characteristic zeolite and phyllosilicate assemblages and with locally occurring hydrothermal overprinting [26, 27, 45].

Long periods of posteruptive thermal history in thick oceanic volcanic sequences are relatively common, and the recorded beginning of alteration starts well after deposition. Rb/Sr ages of celadonite originating from an ODP hole (417A) trace the circulation of hydrothermal fluids through the oceanic crust at least 10 myrs after its formation [77]. Staudigel et al. [78] report celadonite formation from the Troodos massif that lasted between 7 myrs and 19 myrs after oceanic crust formation. The data overlap with obtained Rb/Sr ages in celadonite. Gallahan and Duncan [15] report low-temperature alteration for a longer period of at least >40 myrs after oceanic crust formation in the same area. In the Upper Jurassic-Lower Cretaceous volcano-sedimentary succession of the central Andes in Chile, a time interval between 20 myrs and 25 myrs between volcanism and subsequent burial metamorphism is observed [79]. In the continental flood basalts of the Parana basin, Rb/Sr ages of celadonite (81–107 Ma) are also younger than the eruption age (127-137 Ma) indicating a time interval and a long duration of alteration between eruption and formation of celadonite [80]. Using K/Ar and Rb/Sr data on apophyllite, Ottens et al. [20] determined a time interval of 24 myrs for a late hydrothermal formation of apophyllite from Savda in the Deccan Volcanic Province (India) following burial metamorphism. Środoń et al. [81] report K/Ar ages of celadonite in the 500 m thick Volvyn-Brest Ediacaran continental flood basalts and distinguish two superimposed alteration processes: The Ediacaran hydrothermal alteration event related to meteoric water and the later Caledonian and/or Variscan potassic alteration.

5.2. Linking the New Age Data with the Magmatic Evolution and Sedimentation in the Keweenawan Sequence. In the NSVG, the determined K/Ar ages of celadonite formation are significantly younger than the youngest U/Pb crystallization ages of zircon (1091.61 ± 0.14 Ma) in the Silver Bay intrusion [33]. They are also younger than the youngest reported U/Pb age (1083.52 ± 0.23 Ma) from the Davieaux Island rhyolite in the Michipicoten Island Formation in the eastern part of Lake Superior [33]. Thus, the formation of celadonite is recorded ca. 30 myrs after the emplacement of intrusive units within the NSVG or 20 myrs after the deposition of the Davieaux Island rhyolite.

The celadonite age data in the NSVG also fall within the time window of alteration and copper mineralization in the Portage Lake Volcanics on the Keweenawan Peninsula of Michigan. Bornhorst et al. [82] report Rb-Sr ages of amygdule filling microcline, calcite, epidote, and chlorite that suggest an alteration age of 1060 ± 20 Ma to 1047 ± 20 Ma. The alteration postdates the peak of Portage Lake Volcanics by up to 70 myrs and is considered to be related to burial metamorphism.

The Midcontinent volcanic rocks are overlain in Wisconsin and Michigan by the Oronto Group which includes, from bottom to top, the Copper Harbor Formation, the Nonesuch Formation, and the Freda Formation [83, 84, and references therein] and which in turn are overlain by the Jacobsville Group. According to Symons et al. [85], the Oronto members were oxidized in one major uplift event between about 1063 Ma and 1055 Ma (mean oxidation-magnetization acquisition age of 1060 ± 5 Ma) when regional fluid migration converted the Copper Harbor's gray beds into red beds during the collision of the Grenville Province with the Laurentian Shield. An age of 1060 ± 20 Ma is also reported by Rb-Sr ages of reset biotite in upthrust Archean rocks on the crust-scale fault system of the Montreal River monocline recording thrusting that became active after rifting of the MCR ceased [86]. The youngest celadonite ages fall within the time frame for the youngest detrital zircon ages of 959 ± 19 Ma and of around 1032 Ma of the Jacobsville sandstone [87]. In addition, Rb–Sr isochron dates of 1047 ± 35 Ma and 1020 ± 18 Ma on calcite and chlorite, respectively, from a postore vein at White Pine in the Nonesuch Formation [88, 89] and a Sm–Nd date of 1043 ± 40 Ma for mineralized vein calcites at White Pine [89] are further evidence for regional low-grade metamorphic activity in the MCR. In addition to hydrothermal magmatic activity and burial load, uplift, folding, thrustfaulting, and inversion during the shortening of the Grenvillian collision [36] could also be responsible for fluid migration and alteration.

6. Conclusions

The new age data of celadonite enhance our understanding of the geological evolution of the Midcontinent Rift and provide chronological information for the posteruptive thermal history. The three K/Ar age dates of celadonite (1062 ± 16 Ma, 1039.4 ± 14 Ma, and 955.0 ± 12 Ma) mark the beginning of polyphase metamorphism with a zonal sequence of

characteristic facies assemblages related to later burial load and overprinted by local hydrothermal fluids. The depth-controlled alteration was an ongoing, temporally, and spatially inhomogeneous process starting with the formation of celadonite about 20 myrs after the last record of volcanism in the Midcontinent Rift or about 30 myrs after the emplacement of the aplite in the Silver Bay Complex in the NSVG. The data suggest a time window of >100 myrs for hydrothermal alteration under burial conditions, the longest so far documented in thick continental basaltic sequences. The resulting burial rates are 0.04 km·Ma^{-1} and 0.10 km·Ma^{-1}. Celadonite formed at temperatures below <100°C and is stable up to lower zeolite facies conditions, that is, up to a temperature of approximately 250°C. The oldest celadonite age of 1062 ± 16 Ma may also indicate a minimal eruptive age of the NSVG, which is currently estimated to be in the range of 1091.61 ± 1.5 Ma for the Silver Bay aplite intrusion [33]. The alteration mode changes in space and time within the sequence. It implies the progression of the sequence from a close-to-the-surface alteration mode with input of meteoric water to a burial metamorphic mode. The burial metamorphic mode was further influenced by locally occurring hydrothermal activity due to continuous magmatic activity, large-scale thrusting and possible heat and fluid transfer from the Duluth or Beaver Bay Complexes. The term hydrothermal alteration under conditions of burial metamorphism is suggested to take into consideration the different alteration modes developing within this thick continental flood basalt sequence in space and time during a time window of more than 100 myrs.

Data Availability

All is included in ms.

Additional Points

Highlights. First geochronological data of the posteruptive thermal history of the North Shore Volcanic Group of the Midcontinent Rift in NE Minnesota, USA, the long duration of the thermal history of >100 myrs in a continental flood basalt sequence, K/Ar dating of celadonite, the burial rate, hydrothermal alteration under conditions of burial metamorphism, and zeolite-phyllosilicate assemblages.

Conflicts of Interest

The authors declare no conflict of interest regarding this publication.

Acknowledgments

This project was funded by the Swiss National Science Foundation (grant no. 200021-149232 and grant 2000-37344.9 to STS). STS thanks Radovan Černy (Laboratoire de Cristallographie, Université de Genève) for analyzing the celadonite using synchrotron radiation and for discussion of X-ray data. STS thanks John C. Green, Terry Baerboem, Jim Miller, Mark A. Jirsa (University of Duluth, Minnesota), Karl Seifert (University of Iowa, Ames), Bill Cannon, Laurel Woodruff and Suzanne Nicholson (US Geological Survey), Theodore J. Bornhorst and Bill Rose (Michigan Technological University), and Rick Kollath in Duluth for fruitful discussions of various aspects of the MCR during many field trips, coffee breaks, and conferences. We thank Jean-Marie Boccard (Université de Genève) for the preparation of excellent thin sections, Sam Carmalt for reading the English text, and Lluís and Moritz for their valuable support. The authors highly appreciate the editorial handling by Matthew Steele-MacInnis and are thankful for the helpful and constructive comments of Ömer Bozkaya and Ray Burges, as well as two anonymous reviewers which improved the quality of our manuscript.

References

[1] N. Marks, P. Schiffman, R. A. Zierenberg, and G. O. Fridleifsson, "Hydrothermal alteration in the Reykjanes geothermal system: insights from Iceland deep drilling program well RN-17," *Journal of Volcanology and Geothermal Research*, vol. 189, no. 1-2, pp. 172–190, 2010.

[2] A. J. Andrews, "Saponite and celadonite in layer 2 basalts, DSDP Leg 37," *Contributions to Mineralogy and Petrology*, vol. 73, no. 4, pp. 323–340, 1980.

[3] T. Clayton and R. B. Pearce, "Alteration mineralogy of Cretaceous basalt from ODP Site 1001, Leg 165 (Caribbean Sea)," *Clay Minerals*, vol. 35, no. 4, pp. 719–733, 2000.

[4] G. Giorgetti, P. Marescotti, R. Cabella, and G. Lucchetti, "Clay mineral mixtures as alteration products in pillow basalts from the eastern flank of Juan de Fuca Ridge: a TEM-AEM study," *Clay Minerals*, vol. 36, no. 1, pp. 75–91, 2001.

[5] C. Pflumio, "Evidences for polyphased oceanic alteration of the extrusive sequence of the Semail ophiolite from the Salahi block (northern Oman)," in *Ophiolite Genesis and Evolution of the Oceanic Lithosphere*, T. Peters, A. Nicolas, and R. G. Coleman, Eds., vol. 5 of Petrology and Structural Geology, pp. 313–351, Springer, Dordrecht, 1991.

[6] J. C. Alt, "Very low-grade hydrothermal metamorphism of basic igneous rocks," in *Low-Grade Metamorphism*, M. Frey and D. Robinson, Eds., pp. 169–201, Blackwell Science, Oxford, 1998.

[7] C. Laverne, A. Belarouchi, and J. Honnorez, "Alteration mineralogy and chemistry of the upper oceanic crust from Hole 896A, Costa Rica Rift," in *Proc. ODP, Sci. Results*, J. C. Alt, H. Kinoshita, L. B. Stokking, and P. J. Michael, Eds., vol. 148, pp. 151–170, US Govt. Printing Office, Washington, D.C, 1996.

[8] D. Robinson, S. T. Schmidt, and A. S. de Zamora, "Reaction pathways and reaction progress for the smectite-to-chlorite transformation: evidence from hydrothermally altered metabasites," *Journal of Metamorphic Geology*, vol. 20, no. 1, pp. 167–174, 2002.

[9] G. S. Odin, A. Desprairies, P. D. Fullagar et al., "Nature and geological significance of celadonite," in *Green Marine Clay. Oolitic Ironstone Facies, Verdine Facies, Glaucony Facies and Celadonite Bearing Faciess*, G. S. Odin, Ed., pp. 337–398, Elsevier Publ., Amsterdam, 1988.

[10] G. S. Odin, "How to measure glaucony ages," in *Numerical Dating in Stratigraphy*, G. S. Odin, Ed., pp. 387–403, John Wiley & Sons, Chichester, UK, 1982.

[11] N. Clauer, H. Zwingmann, N. Liewig, and R. Wendling, "Comparative $^{40}Ar/^{39}Ar$ and K–Ar dating of illite-type clay minerals: a tentative explanation for age identities and differences," *Earth Science Reviews*, vol. 115, no. 1-2, pp. 76–96, 2012.

[12] S. Kowalska, A. Wójtowicz, S. Hałas, K. Wemmer, and Z. Mikołajewski, "Thermal history of Lower Palaeozoic rocks from the East European Platform margin of Poland based on K-Ar age dating and illite-smectite palaeothermometry," *Annales Societatis Geologorum Poloniae*, vol. 89, pp. 1–29, 2019.

[13] J. C. Alt, J. Honnorez, C. Laverne, and R. Emmermann, "Hydrothermal alteration of a 1 km section through the upper oceanic crust, Deep Sea Drilling Project Hole 504B: mineralogy, chemistry, and evolution of seawater- basalt interactions," *Journal of Geophysical Research*, vol. 91, no. B10, pp. 10309–10335, 1986.

[14] S. E. Humphris, R. N. Thompson, and G. F. Marriner, "The mineralogy and chemistry of basalt weathering, Holes 417A and 418A," in *Initial Reports of the Deep Sea Drilling Project, LI, LII, LIII, Part 2*, T. Donnelly, J. Francheteau, W. Bryan, P. Robinson, M. Flower, and M. Salisbury, Eds., pp. 1201–1217, Washington (U.S. Government Printing Office), 1980.

[15] W. E. Gallahan and R. A. Duncan, "Spatial and temporal variability in crystallization of celadonites within the Troodos ophiolite, Cyprus: implications for low-temperature alteration of the oceanic crust," *Journal of Geophysical Research*, vol. 99, no. B2, pp. 3147–3161, 1994.

[16] G. Pe-Piper, "Dioctahedral micas in Triassic metavolcanic rocks of western Greece," *The Canadian Mineralogist*, vol. 23, pp. 597–608, 1985.

[17] T. Weisenberger and R. Selbekk, "Multi-stage zeolite facies mineralization in the Hvalfjördur area, Iceland," *International Journal of Earth Sciences*, vol. 98, no. 5, pp. 985–999, 2009.

[18] P. F. Neuhoff, T. Friderikssón, S. Arnorsson, and D. Bird, "Porosity evolution and mineral paragenesis during low-grade metamorphism of basaltic lavas at Teigarhorn, Eastern Iceland," *American Journal of Science*, vol. 299, no. 6, pp. 467–501, 1999.

[19] L. L. Baker, W. C. Rember, K. F. Sprenke, and D. G. Strawn, "Celadonite in continental flood basalts of the Columbia River Basalt Group," *American Mineralogist*, vol. 97, no. 8-9, pp. 1284–1290, 2012.

[20] B. Ottens, J. Götze, R. Schuster et al., "Exceptional multi stage mineralization of secondary minerals in cavities of flood basalts from the Deccan Volcanic Province, India," *Minerals*, vol. 9, no. 6, pp. 351–392, 2019.

[21] M. Mattioli, M. Cenni, and E. Passaglia, "Secondary mineral assemblages as indicators of multi stage alteration processes in basaltic lava flows: evidence from the Lessini Mountains, Veneto Volcanic Province, Northern Italy Period," *Minerals*, vol. 85, pp. 1–24, 2016.

[22] P. J. Loveland and V. C. Bendelow, "Celadonite-aluminous-glauconite: an example from the Lake District, UK," *Mineralogical Magazine*, vol. 48, no. 346, pp. 113–117, 1984.

[23] J. L. Bishop, E. Z. N. Dobrea, N. K. McKeown et al., "Phyllosilicate diversity and past aqueous activity revealed at Mawrth Vallis, Mars," *Science*, vol. 321, no. 5890, pp. 830–833, 2008.

[24] J. C. Green, T. C. Boerboom, S. T. Schmidt, and J. T. Fitz, "The North Shore Volcanic Group: mesoproterozoic plateau volcanic rocks of the Midcontinent Rit System in northeastern Minnesota," in *Archean to Anthropocene. Field Guides to the Geology of the Mid-Continent of North America*, J. D. Miller, G. J. Hudak, C. Wittkop, and P. I. McLaughlin, Eds., pp. 121–146, Geological Society of America, Boulder Colorado, 2011.

[25] S. T. Schmidt, "Alteration under Conditions of Burial Metamorphism in the North Shore Volcanic Group, Minnesota. Mineralogical and Geochemical Zonation," *Heidelberger Geowissenschaftliche Abhandlungen*, vol. 1990, p. 309, 1990.

[26] S. T. Schmidt, "Regional and local patterns of low-grade metamorphism in the North Shore Volcanic Group, Minnesota, USA," *Journal of Metamorphic Geology*, vol. 11, no. 3, pp. 401–414, 1993.

[27] S. T. Schmidt and D. Robinson, "Metamorphic grade and porosity and permeability controls on mafic phyllosilicate distributions in a regional zeolite to greenschist facies transition of the North Shore Volcanic Group, Minnesota," *GSA Bulletin*, vol. 109, no. 6, pp. 683–697, 1997.

[28] J. C. Green, "Geologic and geochemical evidence for the nature and development of the middle proterozoic (Keweenawan) Midcontinent Rift of North America," *Tectonophysics*, vol. 94, no. 1-4, pp. 413–437, 1983.

[29] J. W. Hinze, D. J. Allen, L. W. Braille, and J. Mariano, "The midcontinent rift system: a major Proterozoic continental rift," in *Middle Proterozoic to Cambrian Rifting, Central North America*, R. W. Ojakangas, A. B. Dickas, and J. C. Green, Eds., pp. 7–35, Geological Society of America, Boulder, Colorado, 1997.

[30] S. Stein, C. A. Stein, R. Elling et al., "Insights from North America's failed Midcontinent Rift into the evolution of continental rifts and passive continental margins," *Tectonopysics*, vol. 744, pp. 403–421, 2018.

[31] C. A. Stein, S. Stein, M. Merino, G. Randy Keller, L. M. Flesch, and D. M. Jurdy, "Was the Midcontinent Rift part of a successful seafloor-spreading episode?," *Geophysical Research Letters*, vol. 41, no. 5, pp. 1465–1470, 2014.

[32] P. Bedrosian, "Making it and breaking it in the Midwest: continental assembly and rifting from modeling of EarthScope magnetotelluric data," *Precambrian Research*, vol. 278, pp. 337–361, 2016.

[33] L. M. Fairchild, N. L. Swanson-Hysell, J. Ramezani, C. J. Sprain, and S. A. Bowring, "The end of Midcontinent Rift magmatism and the paleogeography of Laurentia," *Lithosphere*, vol. 9, no. 1, pp. 117–133, 2017.

[34] N. L. Swanson-Hysell, J. Ramezani, L. M. Fairchild, and I. R. Rose, "Failed rifting and fast drifting: Midcontinent rift development, Laurentia's rapid motion and the driver of Grenvillian orogenesis," *Geological Society of America, Bulletin*, vol. 131, no. 5-6, pp. 913–940, 2019.

[35] D. Hutchinson, R. White, W. Cannon, and K. Schulz, "Keweenaw hot spot: geophysical evidence for a 1.1 Ga mantle plume beneath the Midcontinent Rift System," *Journal of Geophysical Research, Solid Earth*, vol. 95, no. B7, pp. 10869–10884, 1990.

[36] W. F. Cannon, "Closing of the Midcontinent rift-a far—field effect of Grenvillian compression," *Geology*, vol. 22, no. 2, p. 155, 1994.

[37] D. W. Davis and J. C. Green, "Geochronology of the North American Midcontinent rift in western Lake Superior and implications for its geodynamic evolution," *Canadian Journal of Earth Sciences*, vol. 34, no. 4, pp. 476–488, 1997.

[38] D. W. Davis and J. B. Paces, "Time resolution of geologic events on the Keweenaw Peninsula and implications for development of the Midcontinent Rift system," *Earth and Planetary Science Letters*, vol. 97, no. 1-2, pp. 54–64, 1990.

[39] D. W. Davis and R. H. Sutcliffe, "U-Pb ages from the Nipigon plate and northern Lake Superior," *Geological Society of America Bulletin*, vol. 96, no. 12, pp. 1572–1579, 1985.

[40] L. M. Heaman and N. Machado, "Timing and origin of midcontinent rift alkaline magmatism, North America: evidence from the Coldwell Complex," *Contributions to Mineralogy and Petrology*, vol. 110, no. 2-3, pp. 289–303, 1992.

[41] S. S. Goldich, A. O. Nier, H. Baadsgaard, J. H. Hoffman, and H. W. Krueger, "The Precambrian Geology and Geochronology of Minnesota," *Bulletin of the Minnesota Geological and Natural History Survey*, vol. 41, p. 193, 1961.

[42] J. C. Green, "Volcanic and sedimentary rocks of the Keweenawan Supergroup in northeastern Minnesota," in *Geology and Mineral Potential of the Duluth Complex and Related Rocks of Northeastern Minnesota*, J. D. Miller Jr., J. C. Green, M. J. Severson, V. W. Chandler, S. A. Hauck, D. M. Peterson, and T. E. Wahl, Eds., pp. 94–102, Minnesota Geological Survey Report of Investigations, 2002.

[43] M. A. Jirsa, "Interflow sedimentary rocks in the Keweenawan North Shore Volcanic Group, northeastern Minnesota," *Minnesota Geological Survey Report of Investigations*, vol. 30, p. 20, 1984.

[44] J. B. Paces and J. D. Miller Jr., "Precise U-Pb ages of Duluth Complex and related mafic intrusions, northeastern Minnesota: Geochronological insights to physical, petrogenetic, paleomagnetic, and tectonomagmatic processes associated with the 1.1 Ga Midcontinent Rift System," *Journal of Geophysical Research: Solid Earth*, vol. 98, no. B8, pp. 13997–14013, 1993.

[45] J. E. Gustavson, *Analysis of porosity evolution during low temperature metamorphism of basaltic lavas and implications for fluid flow, [M.S. thesis]*, University of Florida, 2006.

[46] J. A. Kilburg, *Petrology, structure, and correlation of the Upper Precambrian Ely's peak basalts, [M.S. thesis]*, University of Minnesota–Duluth, Duluth, Minnesota, 1972.

[47] Y.-R. Park and E. M. Ripley, "Hydrothermal flow systems in the Midcontinent Rift: oxygen and hydrogen isotopic studies of the North Shore Volcanic Group and related hypabyssal sills, Minnesota," *Geochimica et Cosmochimica Acta*, vol. 63, no. 11-12, pp. 1787–1804, 1999.

[48] S. T. Schmidt and Z. Sharp, "Oxygen composition of quartz and calcite in amygdules of basalts as evidence of complex alteration history during low temperature-hydrothermal metamorphism," *Mitteilungen der Österreichischen Mineralogischen Gesellschaft*, vol. 141, pp. 203-204, 1996.

[49] S. T. Schmidt and Z. Sharp, "Stable isotope heterogeneity (C, O) in basaltic lava flows of the North Shore Volcanic Group between Duluth and Tofte," *IGCP Project 256, Petrology and Metallogeny of volcanic and intrusive rocks of the Midcontinent Rift System, Duluth, Proceedings*, 1995, pp. 165-166, Duluth, MN, USA, 1995.

[50] J. D. Miller and J. D. Vervoort, "The latent magmatic stage of the Midcontinent rift: a period of magmatic underplating and melting of the lower crust," *Procceedings, Part I: Program with Abstracts. 42nd Annual Insitute on Lake Superior Geology*, 1996, pp. 33–35, Cable, Wisconsin, Minnesota, 1996.

[51] B. Schoene, J. L. Crowley, D. J. Condon, M. D. Schmitz, and S. A. Bowring, "Reassessing the uranium decay constants for geochronology using ID-TIMS U–Pb data," *Geochimica et Cosmochimica Acta*, vol. 70, no. 2, pp. 426–445, 2006.

[52] J. D. Vervoort, K. Wirth, B. Kennedy, T. Sandland, and K. S. Harpp, "The magmatic evolution of the Midcontinent rift: new geochronologic and geochemical evidence from felsic magmatism," *Precambrian Research*, vol. 157, no. 1-4, pp. 235–268, 2007.

[53] G. B. Dalrymple and M. A. Lanphere, *Potassium-Argon Dating: Principles, Techniques, and Applications to Geochronology*, W.H. Freeman and Co., San Francisco, 1969.

[54] K. Wemmer, "K/Ar-Altersdatierungsmöglichkeiten für retrograde Deformations-prozesse im spröden und duktilen Bereich-Beispiele aus der KTB-Vorbohrung (Oberpfalz) und dem Bereich der Insubrischen Linie (N-Italien)," *Göttinger Arb. Geol. Paläont*, vol. 51, pp. 1–61, 1991.

[55] U. Fuhrmann, H. J. Lippold, and J. C. Hess, "Examination of some proposed K–Ar standards: $^{40}Ar/^{39}Ar$ analyses and conventional K–Ar data," *Chemical Geology*, vol. 66, pp. 41–51, 1987.

[56] W. H. Schwarz and M. Trieloff, "Intercalibration of 40Ar–39Ar age standards NL-25, HB3gr hornblende, GA1550, SB-3, HD-B1 biotite and BMus/2 muscovite," *Chemical Geology*, vol. 242, no. 1-2, pp. 218–231, 2007.

[57] R. H. Steiger and E. Jäger, "Subcommission on geochronology: convention on the use of decay constants in geo- and cosmochronology," *Earth and Planetary Science Letters*, vol. 36, no. 3, pp. 359–362, 1977.

[58] V. A. Drits, B. B. Zviagina, D. K. McCarty, and A. L. Salyn, "Factors responsible for crystal-chemical variations in the solid solutions from illite to aluminoceladonite and from glauconite to celadonite," *American Mineralogist*, vol. 95, no. 2-3, pp. 348–361, 2010.

[59] G. Li, D. R. Peacor, D. S. Coombs, and Y. Kawachi, "Solid solution in the celadonite family; the new minerals ferrosceladonite, $K_2Fe_2^{2+}Fe_2^{3+}Si_8O_{20}(OH)_4$, and ferroaluminoceladonite, $K_2Fe_2^{2+}Al_2Si_8O_{20}(OH)_4$," *American Mineralogist*, vol. 82, no. 5-6, pp. 503–511, 1997.

[60] D. A. Reid, "Celadonite and its transformation to smectite in an Entisol at Red Rock Canyon, Kern County, California," *Clays and Clay Minerals*, vol. 36, no. 5, pp. 425–431, 1988.

[61] F. Seifert, "X-ray powder data for Mg-Al celadonite (leucophyllite) from Barcza, Poland," *Contributions to Mineralogy and Petrology*, vol. 19, no. 1, pp. 93–96, 1968.

[62] D. Slovenec, V. Majer, and B. Šebečić, "Aluminium celadonite in tuff from the Strizevo area in western Herzegovina," *Neues Jahrbuch für Mineralogie, Monatshefte*, vol. 8, pp. 363–370, 1995.

[63] W. S. Wise and H. P. Eugster, "Celadonite: s p. ynthesis, thermal stability and occurrence," *American Mineralogist*, vol. 49, no. 7-8, pp. 1031–1083, 1964.

[64] A. P. Zhukhlistov, "Crystal structure of celadonite from the electron diffraction data," *Crystallography Reports*, vol. 50, no. 6, pp. 902–906, 2005.

[65] A. P. Zhukhlistov, B. B. Zvyagin, E. K. Lazarenko, and V. I. Pavlishin, "Krystallografiya," vol. 22, no. 3, p. 498, 1977.

[66] R. C. Reynolds, *NEWMOD®, a computer program for the calculation of basal X-ray diffraction intensities of mixed-layered clays*, R.C. Reynolds, Hanover, 1985.

[67] G. Nicoli, J. F. Moyens, and G. Stevens, "Diversity of burial rates in convergent settings decreased as Earth aged," *Scientific Reports*, vol. 6, article 26359, 2016.

[68] A. Naranjo, J. Horner, R. Jahoda et al., "La Colosa Au porphyry deposit, Colombia: mineralization styles, structural controls, and age constraints," *Economic Geology*, vol. 113, no. 3, pp. 553–578, 2018.

[69] C. D. Henry, H. B. Elson, W. C. McIntosh, M. T. Heizler, and S. B. Castor, "Brief duration of hydrothermal activity at Round Mountain, Nevada, determined from Ar^{40}/Ar^{39} geochronology," *Economic Geology*, vol. 92, no. 7-8, pp. 807–826, 1997.

[70] S. D. Hur, J. I. Lee, J. Hwang, and M. Y. Choe, "K-Ar age and geochemistry of hydrothermal altération in thé Barton Peninsula, King George Island, Antarctica," *Ocean and Polar Research*, vol. 23, no. 1, pp. 11–22, 2001.

[71] W. Bach, B. Peucker-Ehrenbrink, S. R. Hart, and J. S. Blusztajn, "Geochemistry of hydrothermally altered oceanic crust: DSDP/ODP hole 504B-implications for seawater-crust exchange budgets and Sr- and Pb-isotopic evolution of the mantle," *Geochemistry, Geophysics, Geosystems*, vol. 4, no. 3, p. 119, 2003.

[72] J. A. Rodriguez-Losada, J. A. Martinez-Frias, M. A. Bustillo, A. Delgado, A. Hernandez-Pacheco, and J. V. de la Fuente Krauss, "The hydrothermally altered ankaramite basalts of Punta Poyata (Tenerife, Canary Islands)," *Journal of Volcanology and Geothermal Research*, vol. 103, pp. 367–376, 2000.

[73] C. Laverne, P. Agrinier, D. Hermitte, and M. Bohn, "Chemical fluxes during hydrothermal alteration of a 1200-m long section of dikes in the oceanic crust, DSDP/ODP hole 504B," *Chemical Geology*, vol. 181, no. 1-4, pp. 73–98, 2001.

[74] B. Velde, "Celadonite mica: solid solution and stability," *Contributions to Mineralogy and Petrology*, vol. 37, no. 3, pp. 235–247, 1972.

[75] A. M. Miller, A. S. Madden, M. E. Madden, and D. Elmore, "Laboratory-simulated diagenesis of nontronite," *Clays and Clay Minerals*, vol. 60, no. 6, pp. 616–632, 2012.

[76] D. S. Stakes and K. F. Scheidegger, *Temporal variations in secondary minerals from Nazca plate basalts, diabases, and microgabbros*, vol. 154, Memoir Geological Society of America, Kulm, 1981.

[77] S. H. Richardson, S. R. Hart, and H. Staudigel, "Vein mineral ages of old oceanic crust," *Journal of Geophysical Research*, vol. 85, no. B12, pp. 7195–7200, 1980.

[78] H. Staudigel, K. Gillis, and R. Duncan, "K/Ar and Rb/Sr ages of celadonites from the Troodos ophiolite, Cyprus," *Geology*, vol. 14, no. 1, pp. 72–75, 1986.

[79] F. Fuentes, G. Féraud, L. Aguirre, and D. Morata, "$^{40}Ar/^{39}Ar$ dating of volcanism and subsequent very low-grade metamorphism in a subsiding basin: example of the Cretaceous lava series from central Chile," *Chemical Geology*, vol. 214, no. 1-2, pp. 157–177, 2005.

[80] C. Innocent, C. Parron, and B. Hamelin, "Rb/Sr chronology and crystal chemistry of celadonites from the Parana continental tholeiites, Brazil," *Geochimica et Cosmochimica Acta*, vol. 61, no. 17, pp. 3753–3761, 1997.

[81] J. Środoń, O. Kuzmenkova, J. J. Stanek et al., "Hydrothermal alteration of the Ediacaran Volyn-Brest volcanics on the western margin of the East European Craton," *Precambrian Research*, vol. 325, pp. 217–235, 2019.

[82] T. J. Bornhorst, J. B. Paces, N. K. Grant, J. D. Obradovich, and N. K. Huber, "Age of native copper mineralization, Keweenaw Peninsula, Michigan," *Economic Geology*, vol. 83, no. 3, pp. 619–625, 1988.

[83] S. G. Henry, F. J. Mauk, and R. Van der Voo, "Paleomagnetism of the upper Keweenawan sediments: the Nonesuch Shale and Freda Sandstone," *Canadian Journal of Earth Science*, vol. 14, no. 5, pp. 1128–1138, 1977.

[84] S. Baumann, S. Dylka, and D. Malone, "Lithostratigraphic subdivisions of the Mesoproterozoic Copper Harbor Formation (Oronto Group) in Michigan and Wisconsin, USA," *Stratigraphy*, vol. 15, pp. 135–152, 2018.

[85] D. A. Symons, K. Kawasaki, and J. F. Diehl, "Magnetization age from paleomagnetism of the Copper Harbor red beds, Northern Michigan, USA, and its Keweenawan geologic consequences," *Canadian Journal of Earth Sciences*, vol. 56, no. 1, pp. 1–15, 2019.

[86] W. F. Cannon, Z. E. Petermann, and P. K. Sims, "Crustal-scale thrusting and origin of the Montreal River monocline-A 35-km-thick cross section of the midcontinent rift in northern Michigan and Wisconsin," *Tectonics*, vol. 12, no. 3, pp. 728–744, 1993.

[87] D. H. Malone, C. A. Stein, J. P. Craddock, J. Kley, S. Stein, and J. E. Malone, "Maximum depositional age of the Neoproterozoic Jacobsville Sandstone, Michigan: implications for the evolution of the Midcontinent Rift," *Geosphere*, vol. 12, no. 4, pp. 1271–1282, 2016.

[88] J. Ruiz, L. M. Jones, and W. C. Kelly, "Rubidium-strontium dating of ore deposits hosted by Rb-rich rocks, using calcite and other common Sr-bearing minerals," *Geology*, vol. 12, pp. 259–262, 1984.

[89] M. Ohr, *Geochronology of diagenesis and low-grade metamorphism in pelites, [Ph.D. thesis]*, The University of Michigan, Ann Arbor, Michigan, 1993.

[90] J. D. Miller, D. James, J. C. Green, M. J. Severson, V. W. Chandler, and D. M. Peterson, *Geologic map of the Duluth Complex and related rocks, northeastern Minnesota*, Minnesota Geological Survey, Scale 1: 200 000, 2001.

[91] C. A. Stein, J. Kley, S. Stein, D. Hindle, and G. R. Keller, "North America's Midcontinent Rift: when rift met LIP," *Geosphere*, vol. 11, no. 5, pp. 1607–1616, 2015.

[92] S. T. Schmidt and J. C. Green, *Low grade metamorphism of the Keweenawan sequence in Minnesota and Michigan: field trip guidebook for International Symposium "the transition from basalt to metabasalt"*, vol. 294, International Geological Correlation, Programme, Davis, California, 1992.

[93] R. Kretz, "Symbols for rock-forming minerals," *American Mineralogist*, vol. 68, pp. 277–279, 1983.

[94] D. L. Whitney and B. W. Evans, "Abbreviations for names of rock-forming minerals," *American Mineralogist*, vol. 95, pp. 185–187, 2009.